

Magnetic Properties of $\text{Co}_{1-x}\text{Mn}_x\text{Cr}_2\text{O}_4$ Nanoparticles



By

Ehtesham Ali

414-FBAS/MSPHY/S16

Supervised by

Dr. Kashif Nadeem

Assistant Professor (TTS)

Department of Physics

Faculty of Basic and Applied Sciences

International Islamic University,

Islamabad, Pakistan

2018



(K)

Accession No TH 19157

58.07- MS
EHM

- 1- Magnetic Properties
- 2- Quantum methods of magnetism
- 3- Magnetic Susceptibility


Magnetic Properties of $\text{Co}_{1-x}\text{Mn}_x\text{Cr}_2\text{O}_4$ Nanoparticles

By

Ehtesham Ali

(414-FBAS/MSPHY/S16)

This Thesis is submitted to Department of Physics Faculty of Basic and Applied Sciences (FBAS), International Islamic University Islamabad (IIUI) in partially fulfillment of the requirement for the degree of M.S Physics.



CHAIRMAN
DEPT. OF PHYSICS
International Islamic University
Islamabad

Chairman Department of Physics

International Islamic University, Islamabad



Dean Faculty of Basic and Applied Science

International Islamic University, Islamabad

Department of Physics, Faculty of Basic and Applied Sciences

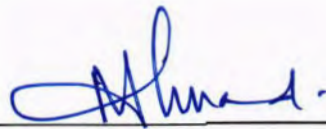
International Islamic University, Islamabad, Pakistan

Final Approval

It is certified that work presented in this thesis entitled “ **Magnetic Properties of $\text{Co}_{1-x}\text{Mn}_x\text{Cr}_2\text{O}_4$ Nanoparticles** ” by **Ehtesham Ali** registration # 414-FBAS/MSPHY/S16 is of sufficient standard in scope and quality for award of degree of MS Physics from Department of Physics, Faculty of Basic and Applied Sciences, International Islamic University Islamabad.

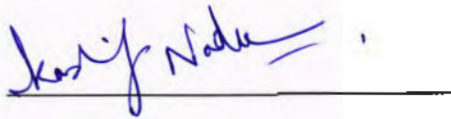
Viva Voce Committee

Chairman

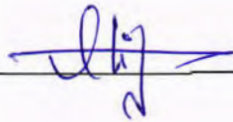


(Department of Physics)

Supervisor



External Examiner



Internal Examiner



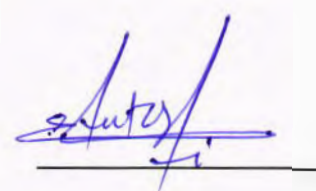


Arabic calligraphy of the Basmala (Bismillah) in a circular, stylized script. The text is written in black ink on a white background. The calligraphy is highly decorative, with thick, flowing lines and sharp, pointed terminals. The words are arranged in a circular pattern, starting from the top and moving clockwise. The first word is 'Bismillah' (In the name of Allah, the Most Gracious, the Most Merciful), followed by 'Ar-Rahman' (The Most Gracious), and 'Ar-Rahim' (The Most Merciful). The script is a form of Thuluth or similar, characterized by its elegant, elongated characters and decorative flourishes.

DEDICATED
TO
MY BELOVED
PARENTS,
RESPECTED
TEACHERS
&
BATCH FELLOWS

Declaration

I Ehtesham Ali (414-FBAS/MSPHY/S16) student of M.S Physics (Session 2016-2018), hereby declare that the work contained in this thesis entitled “**Magnetic Properties of $\text{Co}_{1-x}\text{Mn}_x\text{Cr}_2\text{O}_4$ Nanoparticles**” is my own work and has been generated as the result of my own research. It has not been published or submitted as research work or project/thesis in any form in any university or institute in Pakistan or abroad.



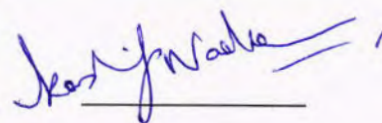
Ehtesham Ali

414-FBAS/MSPHY/S16

Dated: 28.06.2018

FORWARDING SHEET BY RESEARCH SUPERVISOR

This is to certify that the work presented in this research project entitled “ **Magnetic Properties of $\text{Co}_{1-x}\text{Mn}_x\text{Cr}_2\text{O}_4$ Nanoparticles**” has been carried out by **Ehtesham Ali** at Nanoscience and Technology Laboratory, Department of Physics, IIUI. In partial fulfillment of MS (Physics), research has been completed under my guidance and supervision. I am satisfied with the quality of his research work and allow him to submit this thesis for further process to graduate with Master of Science degree from Department of Physics, as per IIUI rules and regulations.



Dr. Kashif Nadeem

Assistant Professor

Department of Physics

International Islamic University

Islamabad

Dated: 28.06.2018

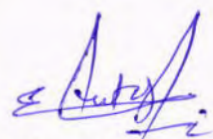
ACKNOWLEDGMENT

First I owe my deepest gratitude to **ALLAH Almighty**, the most Beneficent and the Merciful, who is the source of all knowledge and wisdom, taught us what we knew not. I offer my humblest words of thanks to HIS most noble messenger **Prophet MUHAMMAD** who is forever a torch of guidance and knowledge for all mankind. By virtue of HIS blessings today, I am able to carry out my research work and present it.

I would like to acknowledge the worth mentioning supervision of **Dr. Kashif Nadeem** who gave me the golden opportunity to work on this project, I highly indebted for his inspiring guidance remarkable suggestions constant encouragement, constructive criticism and cooperation during my research work. Without his support and guidance, this research could not have been possible. Moreover, his supervision from the preliminary to the concluding level enabled me to develop an understanding of the field. His wide and deep knowledge have been a great value for me. May **ALLAH Almighty** bless him long life, health, happiness and knowledge.

I express my special thanks to all staff of Physics Department IIUI, for their valuable services. I also express my heartiest thanks to my seniors **Muhammad Kamran, Hur Abbas and Faisal Zeb** for being supportive and cooperative throughout my research work. I also want to thank my colleagues **Zafar Iqbal, Habib ur Rahman and Naman Ahmed Noshahi** for their constant support and courage throughout my research work.

At last but not the least, I forever indebted to my parents and family members Father, Mother, Brothers and Sister for their prayers, continuous support, love, endless patience and encouragement and all other possible help throughout the work. Without their help, understanding this work could not have been completed. I am very grateful to all our friends and class fellows for giving me support, help, encouragement and appreciation in completing this project.



Ehtesham Ali

Table of Contents

Chapter # 1 1

Introduction 1

 1.1 Magnetism 1

 1.2 Brief History Of Magnetism 2

 1.3 Magnetization 2

 1.4 Magnetic Susceptibility 2

 1.5 Types Of Magnetic Materials 3

 1.5.1 Diamagnetism 3

 1.5.2 Paramagnetism 4

 1.5.3 Ferromagnetism 5

 1.5.4 Antiferromagnetism 6

 1.5.5 Ferrimagnetism 7

 1.5.6 Superparamagnetism 8

 1.5.7 Hysteresis Loop 9

 1.6 Nanoscience 10

 1.7 Nanotechnology 10

 1.8 Brief History 11

 1.9 Nanomaterials And Their Types 11

 1.9.1 Zero Dimensional Nanomaterials 12

 1.9.2 One Dimensional Nanomaterials 12

 1.9.3 Two Dimensional Nanomaterials 12

 1.9.4 Three Dimensional Nanomaterials 12

 1.10 Applications Of Nanotechnology 13

 1.11 Chromite 14

 1.11.1 Spinel Chromites 14

 1.11.2 Cobalt Chromite 15

1.11.3 Role of Manganese (Mn) doping in CoCr_2O_4 nanoparticles.....	16
Chapter # 2.....	17
Literature Review.....	17
2.1 Literature review.....	17
Chapter # 3.....	23
Synthesis and Characterization Techniques.....	23
3.1 Synthesis Techniques Of Nanoparticles	23
3.1.1 Top Down Approach.....	23
3.1.2 Bottom Up Approach.....	23
3.2 Synthesis of Manganese Doped Cobalt Chromite Nanoparticles.....	24
3.2.1 Sol-Gel Method.....	24
3.3 Characterization Techniques.....	27
3.3.1 X-rays Diffraction (XRD).....	27
3.3.2 Transmission Electron Microscopy (TEM).....	31
3.3.3 Fourier Transform Infrared Spectroscopy (FTIR).....	32
3.3.4 Superconducting Quantum Interface Device (SQUID) Magnetometer.....	35
Chapter # 4.....	40
Results and Discussion.....	40
4.1 Introduction.....	40
4.2 X-Ray Diffraction.....	42
4.3 Transmission Electron Microscopy.....	45
4.4 Fourier Transform Infrared Spectroscopy.....	45
4.5 Magnetic Properties.....	46
4.5.1 Zero Field And Field Cooled Magnetizations	46
4.5.2 M-H Loops.....	48
Conclusion.....	52
References.....	53

List of Figures

Fig. 1.1. (a) Orbital and (b) spin magnetic moment of electron.....	1
Fig. 1.2. Atomic dipole for diamagnetic material with and without magnetic field.....	3
Fig. 1.3. Response of magnetic susceptibility of diamagnetic materials (a) with applied field and (b) temperature	4
Fig.1.4. Magnetic moment for paramagnetic materials (a) in absence and (b) presence of external magnetic field.....	4
Fig. 1.5. Response of magnetic susceptibility of paramagnetic materials (a) with applied magnetic field and (b) temperature	5
Fig.1.6. Behavior of ferromagnetic domains in (a) the absence and (b) presence of magnetic.....	6
Fig. 1.7. Atomic dipoles in an antiferromagnetic materials without applied magnetic field.....	7
Fig.1.8. Oppositely aligned magnetic moments in ferrimagnetic materials.....	8
Fig.1.9. Atomic dipole ordering in superparamagnet materials.....	8
Fig. 1.10. Hysteresis loop for ferromagnetic material.....	9
Fig. 1.11. Fields of nanotechnology.....	11
Fig. 1.12. Example of nanomaterials.....	13
Fig.1.13. Applications of nanotechnology.....	14
Fig.1.14. Normal spinel structure of chromite.....	15
Fig. 3.1. Top down and bottom up synthesis approach for nanoparticles.....	24
Fig. 3.2. Flow chart for synthesis of cobalt chromite nanoparticles.....	26
Fig.3.3. X-ray tube.....	28

Fig.3.4. Process of inner shell ionization a) incident electron ejects k shell electron from atom b) left a hole in k shell and c) re-arrangement of electron takes place, cause emission of x-ray photon.....29

Fig.3.5. Schematic diagram of x-ray diffraction pattern.....30

Fig.3.6. Diagram of bragg's law.....30

Fig.3.7. Schematic diagram of transmission electron microscope32

Fig.3.8. Diagram of michelson interferometer.....33

Fig.3.9 Constructive interference of two light beams.....34

Fig.3.10. Destructive interference shown by light waves34

Fig.3.11. Schematic diagram of squid.....36

Fig.3.12. Superconducting coil in squid37

Fig.3.13: MPMS Squid.....38

Fig.4.1. (a) XRD patterns of $Co_{1-x}Mn_xCr_2O_4$ nanoparticles43

Fig.4.1 (b) variation in average crystallite size with different concentration of Mn (c) Variation in Lattice constant with different concentration of Mn44

Fig.4.2. TEM Images of $Co_{1-x}Mn_xCr_2O_4$ nanoparticles at (a) 50 nm and (b) 200 nm scale.....45

Fig.4.3. FTIR spectra of $Co_{1-x}Mn_xCr_2O_4$ nanoparticles46

Fig.4.4. ZFC/FC Curves of $Co_{1-x}Mn_xCr_2O_4$ nanoparticles under $H = 50$ Oe field48

Fig.4.5 (a) M-H loops of Mn doped Cobalt chromite nanoparticles at 5K temperature (b) Variation in saturation magnetization with different wt % of Mn in sample50

Fig.4.5 (c) Variation in coercivity with different concentration of Mn in sample.....51

Abstract

The magnetic properties of $\text{Co}_{1-x}\text{Mn}_x\text{Cr}_2\text{O}_4$ nanoparticles with compositions $x = 0, 0.2, 0.4, 0.6, 0.8$ and 1 have been studied in detail. Nanoparticles were characterized by using X-ray diffraction (XRD), transmission electron microscopy (TEM), fourier transform infrared spectroscopy (FTIR) and superconducting quantum interface device (SQUID) magnetometer. XRD patterns showed normal cubic spinel structure with no impurity phase which confirmed single phase formation of $\text{Co}_{1-x}\text{Mn}_x\text{Cr}_2\text{O}_4$ nanoparticles. Crystallite size revealed increasing trend from 36 to 47 nm with increasing concentration of Mn and maximum value was for MnCr_2O_4 nanoparticles (47 nm). FTIR spectra confirmed the formation of single phased cubic spinel structure of these nanoparticles. ZFC/FC curves were taken under 50 Oe field. CoCr_2O_4 nanoparticles showed paramagnetic to long range ferrimagnetic phase transition at $T_C = 100$ K, ferrimagnetic phase changes into conical spin spiral state at $T_S = 30$ K and appearance of lock-in transition state at $T_L = 10$ K. These magnetic transitions T_C , T_S and T_L shifted to lower temperature with increasing concentration of Mn and after $x = 0.2$ concentration, the T_S and T_L completely suppressed. CoCr_2O_4 nanoparticles with $x = 0$ and 0.2 concentration of Mn revealed negative magnetization due to uncompensated spins at grain boundaries which gets suppressed with the increasing concentration of Mn. M-H loops of $\text{Co}_{1-x}\text{Mn}_x\text{Cr}_2\text{O}_4$ nanoparticles were taken at 5 K. Saturation magnetization of these nanoparticles increased with Mn doping which is attributed to large magnetic moment of Mn as compared to Co. In summary, Mn doping affected efficiently the magnetic properties of CoCr_2O_4 nanoparticles and enhanced magnetization due to large ionic radii and higher value of magnetic moment of Mn.

Chapter 1

Introduction

1.1 Magnetism

An electron has two basic attributes "Spin" and "Charge". Phenomena of Magnetism in a material arises because of motion of electron in an atom around the nucleus. An electron has two types of motion in an atom i.e, orbital motion and spin motion. Electrons motion around the nucleus is called as orbital motion of electron while motion of electron that it possess around its own axis is termed as spin motion of electron as shown in Fig. 1.1. Magnetic moment generated by the motion of electron around the nucleus is much less as compared to spin motion of electron. Net magnetization produced in a material is considered to be as the combined effect of magnetization produced due to spin and orbital motion of electron. If there exist exchange coupling between the magnetic moment produced by neighboring atoms, a magnetic order may form in a material. If all the magnetic moments in an atom are aligned in one direction then exchange coupling is positive and if the magnetic moments are antiparallel to each other than the exchange coupling is negative.

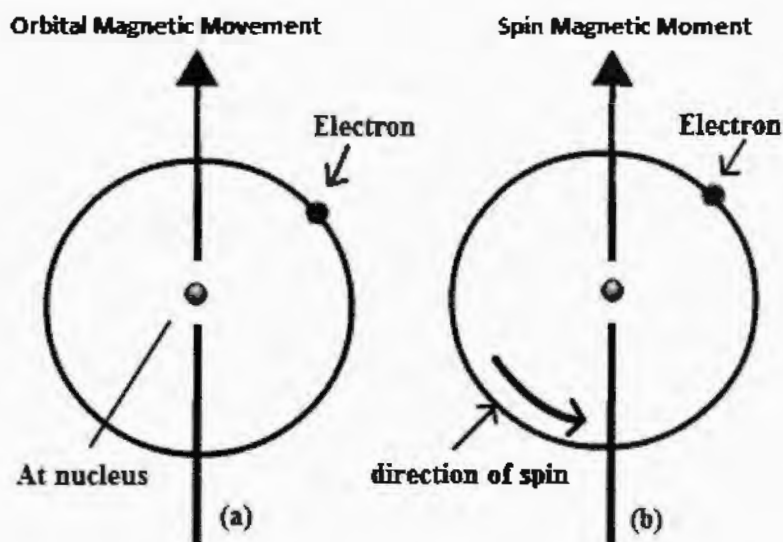


Fig. 1.1: (a) Orbital and (b) spin magnetic moment of electron [1].

Initially, all the magnetic moments inside the material are randomly oriented and have no net magnetization. While in externally applied magnetic field, all the randomly aligned magnetic moment directed in the direction or opposite to the applied magnetic field. The feedback of magnetic moments toward externally applied field depends on the type of material [2].

1.2 Brief history of magnetism

Study on magnetism started with the discovery of a mineral called magnetite (Fe_3O_4). Magnetite is considered to be the first magnetic material. Huge amount of magnetite have been found in the district of magnesia which is now the part of Turkey. Word magnet comes out from a Greek word said to come from that district name. The first logical investigation on magnetism was done by William Gilbert who wrote his book "On the Magnet" in 1600 [3].

1.3 Magnetization

Magnetization in a material can be defined as, magnetic dipole moment per unit volume in a material. Mathematical expression used for magnetization M is,

$$M = m/V \quad (1.1)$$

Where m = magnetic dipole moment, V = volume of material. Magnetization in a material is measured in amperes per meter (Am^{-1}) [4].

1.4 Magnetic susceptibility

This term refers that if a small magnetic field is exerted on a material, a small magnetic effect is produced in the material in the same direction as the external field [5]. Mathematically it can be expressed as,

$$\chi_m = M/H \quad (1.2)$$

or,
$$M = \chi_m H \quad (1.3)$$

Where " χ_m " is the magnetic susceptibility 'M' is the magnetization produced in a material and 'H' is the applied magnetic field.

$\chi < 1$ for diamagnetic material,

$\chi = 1$ for paramagnetic material,

$\chi > 1$ for ferromagnetic material.

Where, measuring unit of χ_m is emu/g/Oe [6].

1.5 Types of magnetic materials

Different type of materials respond differently to the externally applied magnetic field because of the different type of exchange interaction between the magnetic moments of an atom. Due to this different type of response produced by the materials. Magnetic material are classified in to the different types which are explained below:

1.5.1 Diamagnetism

Diamagnetic effect is present in every material. In 1847 it was first observed by Michael Faraday. Diamagnetic phenomena in a material takes place because of motion of electron around the nucleus in an atom. When an external \mathbf{B} field is applied on the diamagnetic material, electrons present in the atomic orbitals act against the field in order to produce induced magnetic moment which will further oppose the applied magnetic field. Due to this effect material is repelled in the magnetic field. Magnetic moments of diamagnetic material tends to be in opposite direction to the applied magnetic field as shown in Fig. 1.2. Examples of such materials are mercury (Hg), Water (H_2O), Bismuth (Bi), Antimony (Sb) etc.

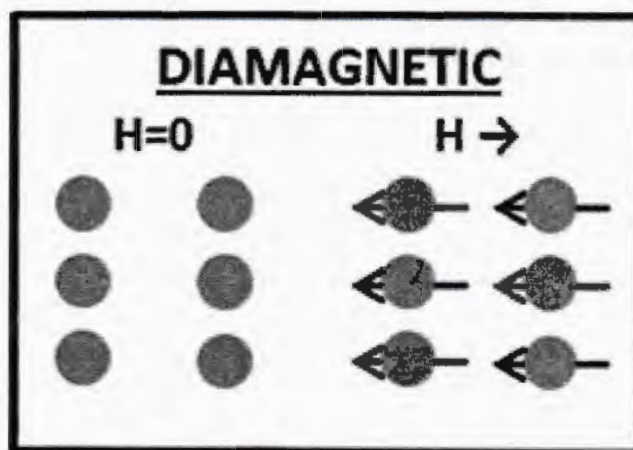


Fig. 1.2: Atomic dipoles for diamagnetic material with and without magnetic field [7]

Susceptibility of diamagnetic material is negative as shown in Fig. 1.3 (a) while increase in temperature causes no change in magnetic susceptibility and it remains constant as shown in Fig. 1.3 (b) [8].

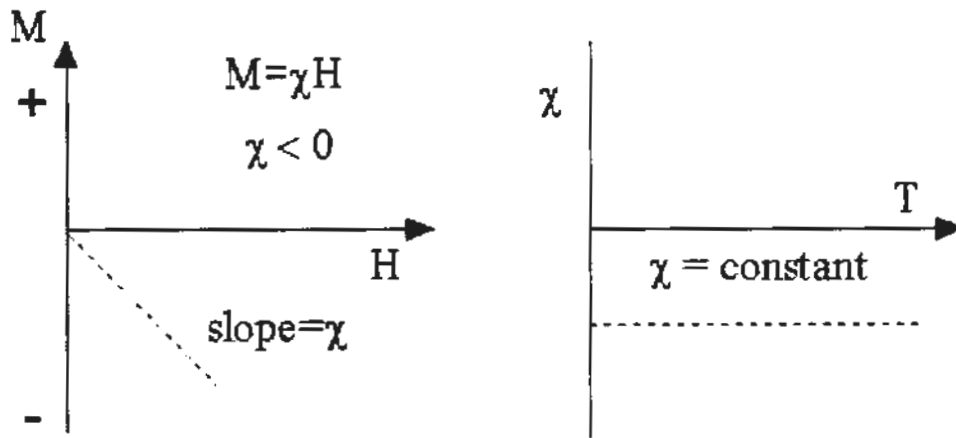


Fig. 1.3: Response of magnetic susceptibility of diamagnetic material (a) with applied field and (b) temperature [1].

1.5.2 Paramagnetism

Paramagnetic materials are those materials that shows attraction toward externally applied magnetic field. In the absence of external magnetic field these materials show no net magnetic moment. In paramagnetic materials, adjacent magnetic moments are randomly oriented to each other but in the presence of external magnetic field they produce internal induce magnetic field parallel to that of applied magnetic field as shown in Fig. 1.4. When external magnetic field is removed, these materials show zero net magnetization. Paramagnetism arises due to the presence of unpaired electrons in an atom. Paramagnetic materials show positive susceptibility [9].

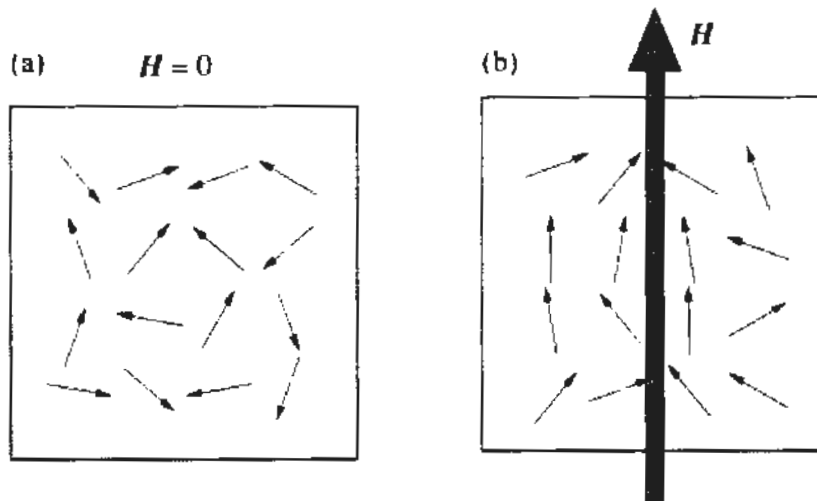


Fig. 1.4: Magnetic moment for paramagnetic materials (a) in absence and (b) presence of external magnetic field [10].

Magnetization effect produced by paramagnetic materials decreases with increasing temperature. Due to thermal agitation, magnetic moments of material gets disturbed hence decreasing the net magnetization of paramagnetic material. Dependence of paramagnetic susceptibility on the temperature is described by using the relation,

$$\chi = \frac{C}{T} \dots\dots\dots(1.4)$$

Eq 1.3 is called the Curie Law of paramagnetism, C is called the Curie constant [11]. Example of paramagnetic material are magnesium, molybdenum and lithium etc. Susceptibility of Paramagnetic material is positive as shown in Fig. 1.5 (a) with the increasing magnetic field, magnetization of the material also increases linearly. While the temperature has inverse effect on the susceptibility, increase in temperature causes no change in magnetic susceptibility and it remains constant as shown in Fig. 1.5 (b).

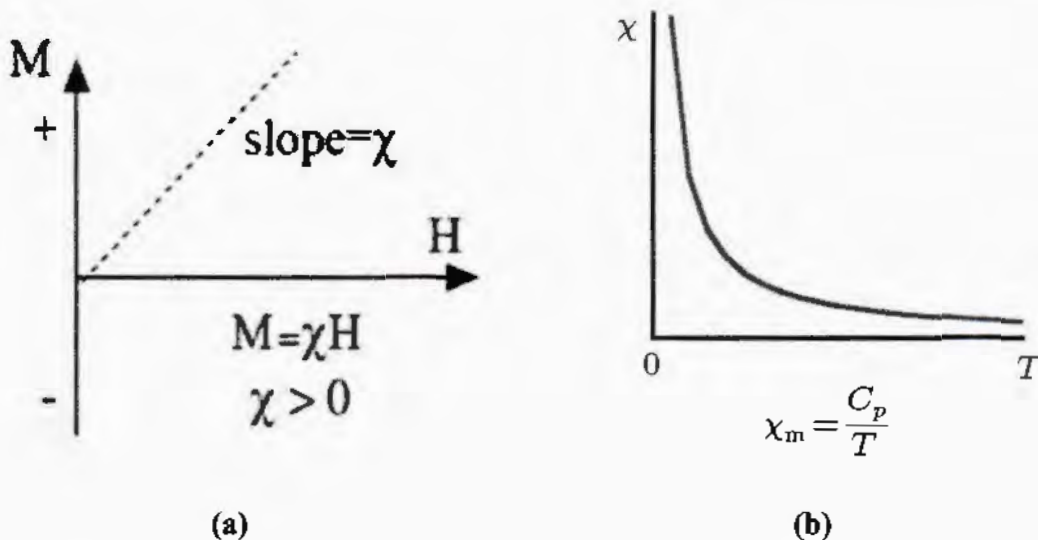


Fig. 1.5: Response of magnetic susceptibility of paramagnetic materials (a) with applied magnetic field and (b) temperature [12].

1.5.3 Ferromagnetism

In ferromagnetic materials, there exists magnetic domains. Each magnetic domain consists of 10^{12} to 10^{16} atoms. Magnetic dipole moments in each magnetic domain are parallel to each other without applying external magnetic field. Initially these magnetic domains are randomly aligned with respect to one another but when external magnetic field they gets themselves aligned in the direction of external magnetic field. Ferromagnetic materials remain magnetized even in zero magnetic field. This phenomenon is known as

spontaneous magnetization [13]. Over lapping of wave function takes place in ferromagnetic material which the main cause of spontaneous magnetization in these type of materials [14]. Fig. 1.6 (a) represents the randomly aligned ferromagnetic domains when no external magnetic field is applied and Fig. 1.6 (b) shows parallel aligned ferromagnetic domains when external magnetic field is applied.

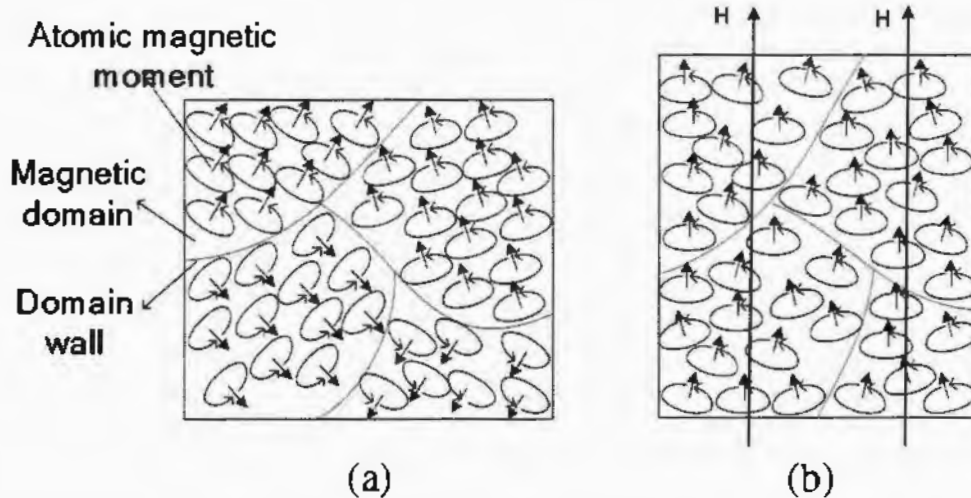


Fig. 1.6: Behavior of ferromagnetic domains in (a) the absence and (b) presence of magnetic field [15].

When the temperature of ferromagnetic material is increased, disordering of magnetic domains takes place due to thermal agitation inside the material and at a certain temperature ferromagnetic materials changes into paramagnetic material. Temperature at which ferromagnetic material changes into paramagnetic material is called Curie Temperature (T_c). Relation used for ferromagnetic susceptibility is [16],

$$\chi = \frac{C}{T - T_c} \dots\dots\dots(1.5)$$

Curie temperature of nickel is $\sim 650^\circ\text{C}$ [17].

1.5.4 Antiferromagnetism

In Antiferromagnetic material, magnetic moment are oriented in opposite direction having equal magnitude. In antiferromagnetic material, acquired magnetization is zero when no external **B** field. While in the presence of external magnetic field, alignment of magnetic moments takes place and antiferromagnetic material changes into ferromagnetic state called Field Induced ferromagnetism. Phenomena of Antiferromagnetism takes place at low temperature called Neel Temperature [18]. Fig. 1.7 shows the clear picture of the

atomic dipoles in an antiferromagnetic material in the absence of externally applied magnetic field.

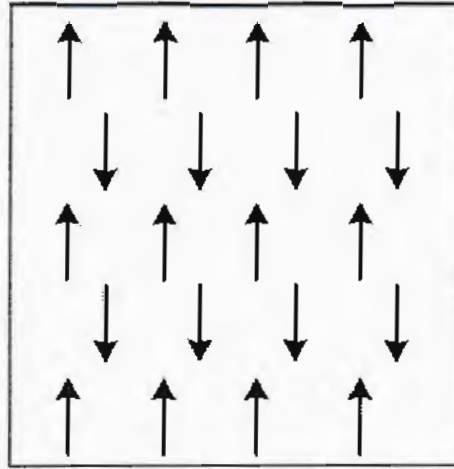


Fig. 1.7: Atomic dipoles in an antiferromagnetic materials without applied magnetic field [19].

1.5.5 Ferrimagnetism

In Ferrimagnetic material, magnetic moment of adjacent atoms are aligned in opposite direction and have unequal magnitude due to which these type of material acquire net magnetization even in zero external magnetic field [20]. This type of magnetization is called “spontaneous magnetization”. But when external magnetic field is applied to ferrimagnetic material, oppositely aligned magnetic moments tends to align themselves along the direction of applied magnetic field. Hence showing the phenomena of field-induced ferromagnetism. Being temperature dependent, ferrimagnetism is dominant in a material at low temperature. At higher temperature, these type of material changes into paramagnetic material. Temperature at which ferrimagnetic state of material change into paramagnetic is called the “Neel temperature”. Ferrimagnetic material with oppositely aligned magnetic moments are in shown in Fig. 1.8. Ferrite is the typical example of Ferrimagnetic material [21].

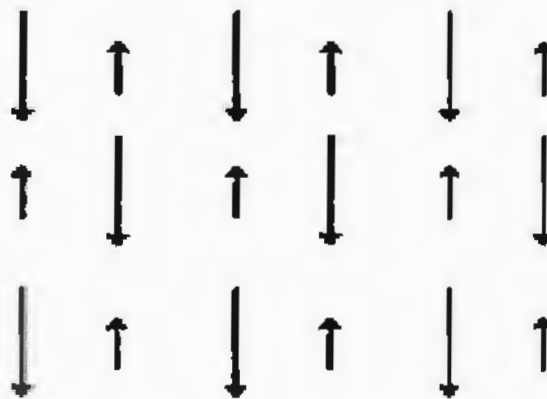


Fig. 1.8: Oppositely aligned magnetic moments in ferrimagnetic materials [22].

1.5.6 Superparamagnetism

Superparamagnetism is a single domain phenomena in which magnetic moment of nanoparticle is taken into account instead of atom. Generally nanoparticle is larger than atom so there is strong exchange interaction takes place between the electrons of these substance showing strong magnetization when external magnetic field is applied. These materials exhibit a minute effect of induced magnetization. In terms of magnetic susceptibility, these type of materials lies between paramagnetic and ferromagnetic material [23]. The arrangement of atomic dipole ordering in superparamagnet materials are revealed in Fig. 1.9.

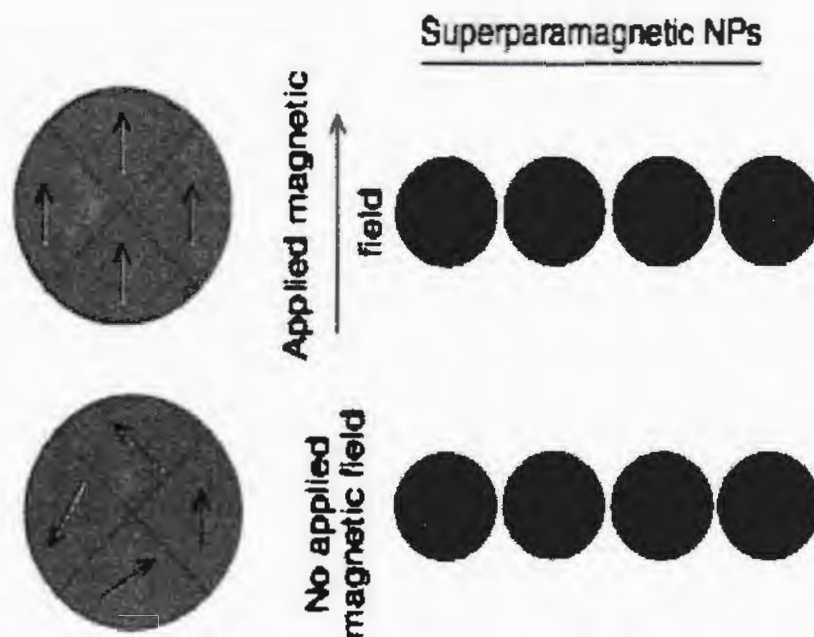


Fig. 1.9: Atomic dipole ordering in superparamagnet materials [24].

1.5.7 Hysteresis loop

Hysteresis is a Greek work which means “to lag behind or having deficiency”. In a ferromagnetic material, there exist magnetic domains in which magnetic moments are aligned in same direction with in one domain but are randomly oriented with respect to other magnetic domains. Fig. 1.10 shows the hysteresis loop of ferromagnetic materials. In hysteresis loop, magnetization of material is related to applied magnetic field [25]. Initially when magnetic field is applied, domains inside ferromagnetic material start's alligning themselves in the direction of external magnetic field hence increasing the magnetization. A point comes when magnetization of material do not increase further by the increase of magnetic field. This value of magnetization is called saturation magnetization (M_s).

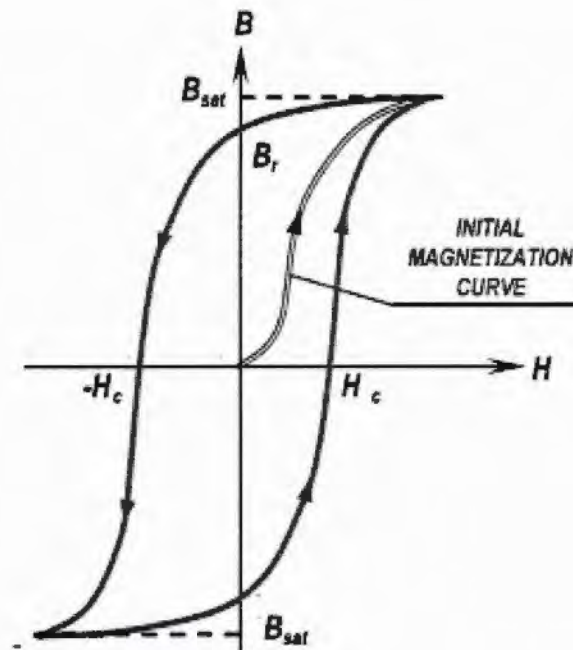


Fig. 1.10: Hysteresis loop for ferromagnetic material [26].

When we start decreasing the magnetic field it do not follow the same path as for increasing magnetic field. While decreasing the magnetic field magnetization of material do not get zero, this happen due to the fact that magnetic domains are strongly coupled to each other. This magnetization is referred as remanence magnetization of material. To get zero magnetization in material, magnetic field is applied in the reverse direction. Hence, material become demagnetized and this demagnetizing field is called as coercive field (H_c).

Area of loop tells us about how much energy is being dissipated in magnetizing and demagnetizing the material. If area of a loop of material is large, it means it will be hard to get aligned the magnetic domains in the direction of applied magnetic field and hence to magnetize the material but once the material will be magnetized, it will become hard enough to demagnetize the material. These type of material are called as "Hard Magnets". While on the other hand, if a material has small area of loop, these type of material will be easy to magnetize it means, magnetic domains will be easily get aligned in the direction of external magnetic field, but they are very easy to demagnetize too. These type of material are called as "Soft Magnets". Hard magnets are more suitable for data storage than a soft magnet.

1.6 Nanoscience

Nanoscience is the branch of science that studies and transforms matter into atomic, molecular and supramolecular state (on nanometer scale) [27]. At such a small length, surface boundary effects become dominant that presents the properties of material that are not identified on larger length scale.

1.7 Nanotechnology

Nanotechnology is the technology conducted at the nano scale. "Nanotechnology deal with those materials whose structures show unique physical, chemical and biological properties, because of their nanoscale size". One nanometer is a billionth part of a meter [28]. Word Nano is derived from Greek language which means little. One nanometer is a length equal to the length of 10 hydrogen atoms, placed in a line. Nanotechnology involves in every field it almost changed the various fields of life particularly it involved in gadgets, sensor innovation, industry and so on [27]. Nanomaterials are not new, nor they first created by man. To give an idea of nanomaterial, DNA being a building block of every living thing is few nanometer wide. There are many natural resources of nanomaterials e.g, catalyst, soot particles, certain minerals etc. New thing is that we can now examine and partially control these particles. Materials at the nanometer scale range show remarkable different properties as compared to their bulk counterpart. Small features allows more functionality in a given space, nanotechnology is not just a basic continuation of scaling down from micron meter scale down to nanometer scale but it gives totally different

properties of a material because of quantum confinement effect of electron. Soft carbon in the form of graphite become stronger than steel. Aluminum become combustible when particle size is reduced to nanometer scale. Nanotechnology is concerned with almost all areas of physical science which are serving human being. Nanotechnology is involved in every branch of science like physics, chemistry, biology, material science etc. Nanotechnology is playing vital role in various fields of life briefly shown in the Fig. 1.11.

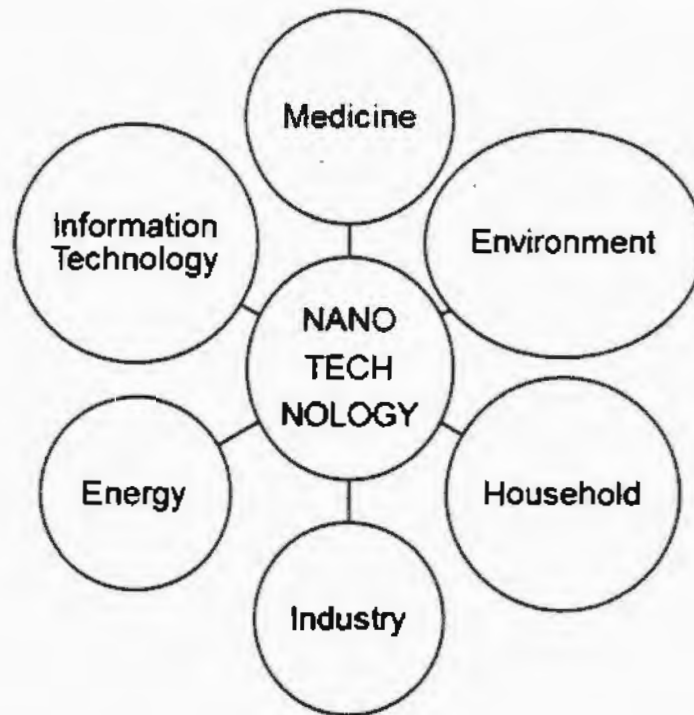


Fig. 1.11: Fields of nanotechnology [27].

1.8 Brief history of nanotechnology

In 1974 "Nori taniguchi" introduced the term Nanotechnology. He uses this word to depict ultrafine machining. The basic concept of nanotechnology was discussed by a famous Professor Richard Feynman, professor at Californian institute of technology. He said that "There is plenty of depth at the bottom" [29].

1.9 Nanomaterials and their types

Nanomaterials are described as the materials whose minimum one dimension is found within the range of 1-100 nm scale range [30]. A nanomaterial is an item that has no less than one measurement in the nanometer scale. Nanomaterials show novel characteristics such as increased strength, corrosion resistant, chemically active or

conductivity [31]. Nanomaterials have the ability to improve the life quality and to contribute to industrial competitiveness.

There are four type of nanomaterials depending upon the degree of confinement of electron which are briefly discussed below:

1.9.1 Zero dimensional nanomaterials

In zero dimensional nanomaterial, all dimension of materials lies in nano scale range 1 – 100 nm. Nanomaterials are most representation of zero dimensional materials. In zero dimensional nanomaterials, quantum confinement takes place in all three dimensions.. Quantum dot are the examples of zero dimensional nanomaterial.

1.9.2 One dimensional nanomaterials

In one dimensional nanomaterials, two dimensions of material lie within the nano range scale while only one dimension lie outside the nano range scale (1-100 nm). In one dimensional nanomaterials, quantum confinement takes place in two dimensions while electron is free to move in one dimension. Example of one dimensional nanomaterials are nanowires and nanotubes.

1.9.3 Two dimensional nanomaterials

In two dimensional nanomaterials, only one dimension of a material lie with in the nano range scale while other two dimension are outside this nano scale range. In two dimensional nanomaterials, quantum confinement takes place in one dimensions while electron is free to move in two dimensions. Graphene, Thin film is an example of two dimensional materials.

1.9.4 Three dimensional nanomaterials

In three dimensional material, all the dimension of a material lie outside the nano range scale. These materials are greater than 100 nm in all dimensions. In three dimensional nanomaterials, no quantum confinement of electron takes place while electron is free to move in all dimension of nanomaterial. Example of three dimensional materials is polycrystals.

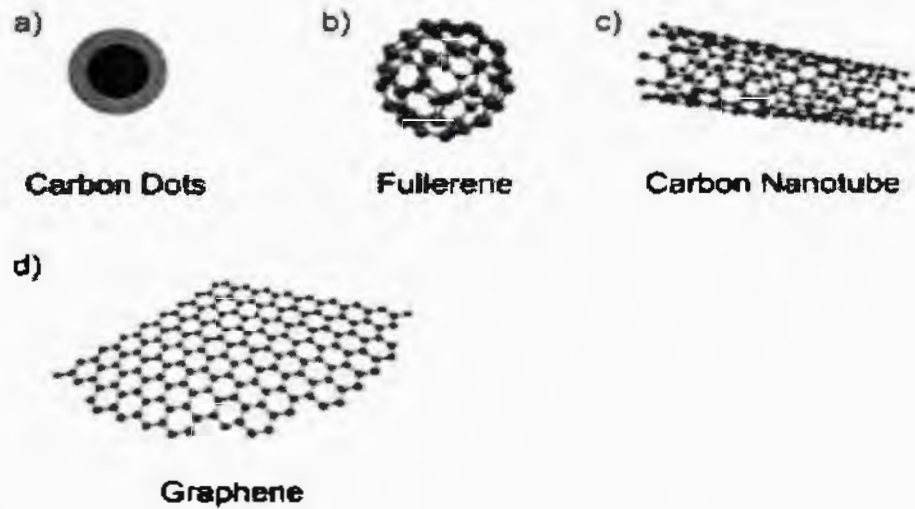


Fig. 1.12: Example of nanomaterials [32].

1.10 Applications of nanotechnology

Being an interdisciplinary field nanotechnology found its application almost in every field. Various applications of nanotechnology in different fields are shown in Fig. 1.13 and some of them are given below;

Medical:	Cancer Treatment, Antibacterial agent, Antimicrobial coating,
Electronics:	Nano Diodes, Single Electron Transistor, Hard disk.
Consumers:	Self-cleaning glass, Lightweight materials, Nano gloves,
Industrial coatings:	Environmental coatings, magnetic coatings.
Aerospace:	Low weight composites, thruster and body materials.
Automotive:	Nano-clear coats, Polymer glasses, Spark plug.
Power:	Battery, solar cell, Fuel cell [33].

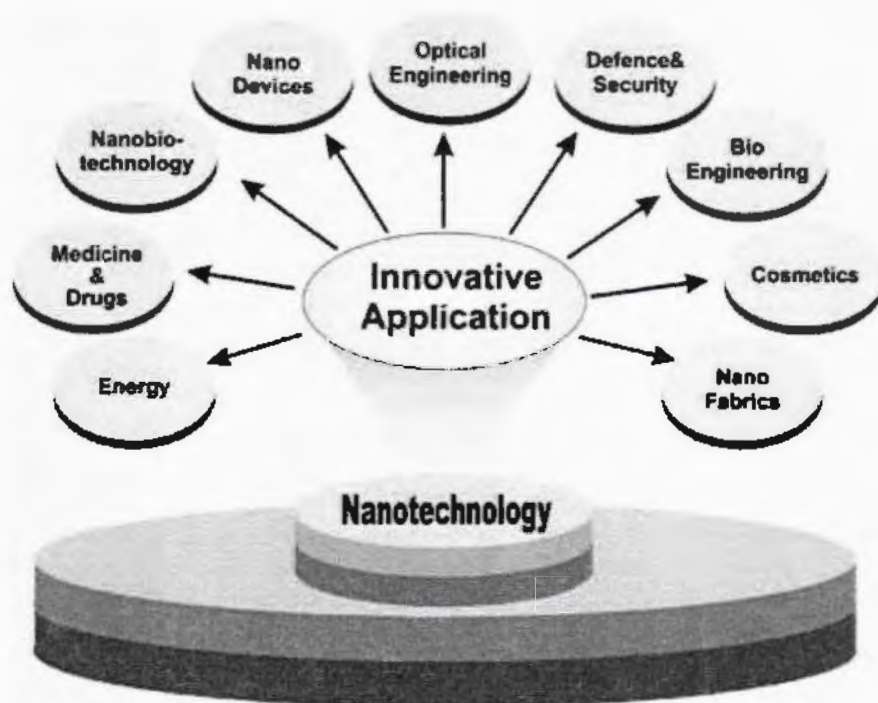


Fig. 1.13: Applications of nanotechnology [33].

1.11 Chromite

Chromites are mixed-metal oxides having general formulae AB_2O_4 where A and B represents the divalent and trivalent cations. Chromites are normal spinel compound in which Co^{2+} ion occupy tetrahedral while Cr^{3+} occupies octahedral site [34].

1.11.1 Spinel chromites

Spinel chromite have general formula $[A^{2+}B_2^{3+}O^{2-}]$ and it consists of divalent and trivalent cations while a divalent negatively charged oxygen ion also present in it. A^{2+} is a divalent while B_2^{3+} is trivalent cation. A divalent cation represents tetrahedral lattice site in crystal structure and trivalent cation occupies octahedral lattice site in the unit cell. Unit cell of spinel chromite consists of 8 divalent metal cation, 16 trivalent metal cation (Chromium) and 32 oxygen ions. The partial part of unit cell of spinel structure of chromite is shown in Fig. 1.14. Different type of exchange interaction may take place between the two lattice sites (tetrahedral and octahedral). The interaction may be such as between tetra-tetra, tetra-octa, octa-tetra and octa-octa lattice site while the strongest interaction is between tetra-octa lattice sites [35].

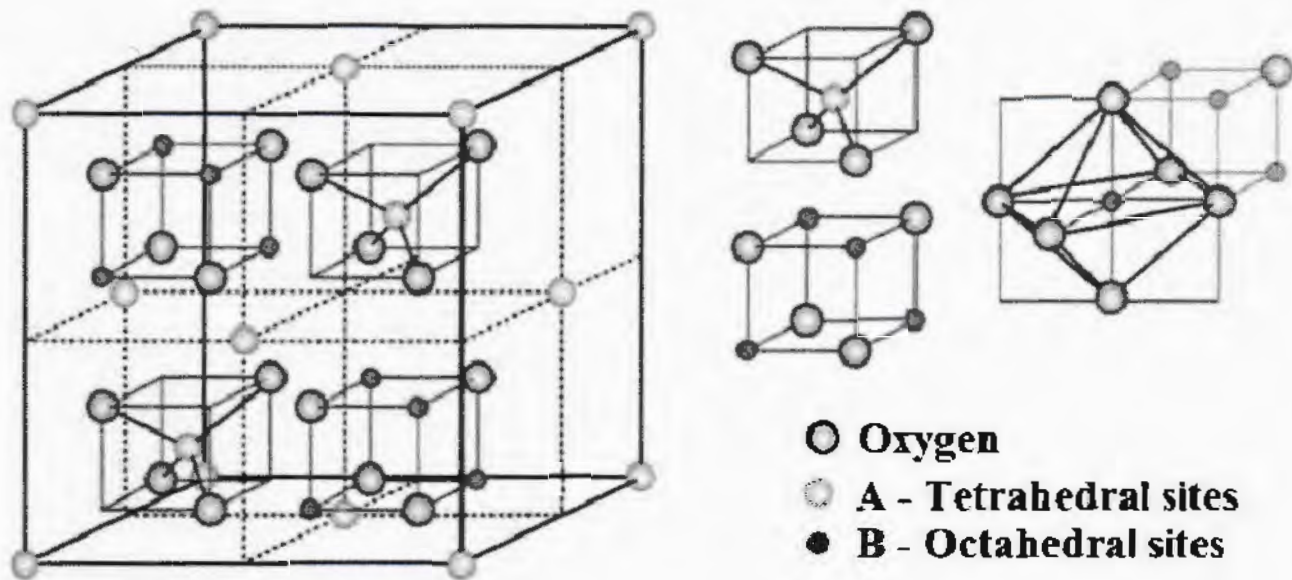


Fig. 1.14: Spinel structure of chromite [36].

1.11.2 Cobalt chromite

CoCr_2O_4 , an insulating normal spinel compound. These nanoparticles are ferrimagnetic in nature [37]. CoCr_2O_4 nanoparticles gains importance due to most striking property as multiferroic materials [38]. At the same temperature ferroelectric and ferromagnetic states coexist in multiferroic materials [35]. Coexistence of these two states is of great importance. Phase transitions takes place in CoCr_2O_4 nanoparticles at different temperature range. Different phase transition take places in multiferroic material from paramagnetic to ferrimagnetic state by further lowering the temperature it enters into the long range spiral order and then in lock-in transition state. In long range spiral ordering, spin of nanoparticles lie on the conical surfaces. Also spiral component induces polarization of electric charges and spontaneous magnetization that's why chromite are called as multiferroic material. Ferrimagnetic state has long range order at low temperature range and it also causes a spontaneous magnetization of about $0.3\mu_B$ [39]. CoCr_2O_4 nanoparticles is used in ceramic materials, heat resistant pigment, high density magnetic memory media, telecommunication systems, electromagnetic sensors etc.

1.11.3 Role of manganese (Mn) doping in CoCr_2O_4 nanoparticles

CoCr_2O_4 being multiferroic material shows ferroelectric and ferromagnetic states at same phase. Being a transition metal, Mn has partially filled 'd' orbital due to which it will tend to follow the Jahn teller effect and will cause to change the crystal structure of CoCr_2O_4 nanoparticles. Doping of Mn will affect the physical properties as well as magnetic properties of CoCr_2O_4 . Ionic radii of 'Mn' is greater than 'Co' which will cause change in crystallite size and it will also tend to change the cationic distribution of ions with in the crystal structure of CoCr_2O_4 nanoparticles due to its larger ionic radii. CoCr_2O_4 also exhibit different magnetic phase transitions at different temperatures such as T_C , T_S and T_L . As an independent material "Mn" behave as paramagnetic material which will cause the change in these magnetic transition temperatures. It will also control the particle size, magnetic properties such as magnetic phase transition temperature, magnetization and coercivity of particles.

Chapter 2

Literature Review

2.1 Literature review

Ptak *et al.* [40] studied the temperature-dependent magnetic properties of CoCr_2O_4 nanoparticles containing size of 23 and 4 nm. In bulk CoCr_2O_4 , ferrimagnetic magnetic transition takes place around $T_C = 97$ K. Reducing the particles size has affected the magnetic transition temperature. Critical temperature (T_C) reduce to about 93 K for 23 nm and 75 K for 4 nm particles. For nanoparticles of 23 nm, incommensurate spiral magnetic order takes place at $T_S = 24$ K. IR studies has shown unusual behavior at temperature lower than T_C which is due to strong exchange interaction between low wavenumber phonon and ferrimagnetic component of magnetic order.

Lei *et al.* [41] synthesized CoCr_2O_4 nanosheets by ethylene glycol in situ reduction metod. X-ray diffraction pattern confirmed the cubic spinel structure of prepared samples. Diameter of CoCr_2O_4 nanosheets was found between 20 – 30 nm by using electron microscopy. Magnetic measurements revealed that long range ferrimagnetic transitions takes place at critical temperature at $T_C = 86$ K along with two magnetic transitions such as spiral magnetic state occurs at $T_S = 20$ K and lock-in transition at $T_L = 13$ K. Magnetic results were consisted with results obtained through specific heat measurement of these nanosheets.

Melot *et al.* [42] investigated the magnetic properties of $\text{Zn}_{1-x}\text{Co}_x\text{Cr}_2\text{O}_4$ nanoparticles. They have shown that by replacing non-magnetic ion (Zn) to magnetic ion (Co), different magnetic phase transitions has been observed. At low concentration of Co in ZnCr_2O_4 , transition from antiferromagnets to glassy magnetism is observed. At higher concentration of Co, ferrimagnetic and conical ground states are observed. Magnetic transitions are observed due to the self coupling between nearest neighbors and also due to the interaction of atoms placed at different lattice sites in a unit cell.

Lu *et al.* [43] synthesized spinel $\text{Mn}_{1+x}\text{Cr}_{2-x}\text{O}_4$ nanoparticles where ($0 \leq x \leq 1$). Lattice parameters was found to be increased with increasing concentration of Mn up to

$x = 0.7$. At concentration higher than $x = 0.7$, symmetry of crystal changed from cubic to tetragonal due to John-teller distortion but it is consistent with increase of lattice parameters of doped structure.

Chang *et al.* [44] studied spin conical phase transitions in bulk CoCr_2O_4 at temperature lower than 40 K. The incommensurate propagation vector observed at 26 K which represents spin spiral state and this vector fixed commensurately at 14.5 K which represents another magnetic state in CoCr_2O_4 . These magnetic transitions belong to long range ferrimagnetic order which was identified by the width of magnetic peaks. This newly identified magnetic transition will cause to give new properties of multiferroic material.

Kamran *et al.* [35] reported the influence of SiO_2 coating on magnetic properties of CoCr_2O_4 nanoparticles. Crystallite size was found in the range of 19-28 nm. Average crystallite size and lattice parameters start decreasing with the increasing concentration of SiO_2 in cobalt chromite nanoparticles. Zero Field cooled/Field Cooled curve showed that nanoparticles undergo a phase shift from paramagnetic state to ferrimagnetic state when the temperature is decreased from 101 to 95 K. At $T_S = 27$ K, a conical state is observed in all samples and decreases with decreasing concentration of crystallite size. By further lowering the temperature Lock-in transition state appeared in the uncoated sample. Other magnetic parameters such as temperature dependent AC-susceptibility, saturation Magnetization and broadening of T_C peak also decrease due to the increasing concentration of SiO_2 nanoparticles.

Kamran *et al.* [34] studied the magnetic properties of $\text{Co}_{1-x}\text{Mg}_x\text{Cr}_2\text{O}_4$ nanoparticles with the composition from $x = 0.0$ to $x = 1$. XRD pattern reveals the spinel structure for all the samples. No single impurity was found in the samples by using Rietveld refinement analysis of XRD which signifies the single phase of $\text{Co}_{1-x}\text{Mg}_x\text{Cr}_2\text{O}_4$ nanoparticles. FTIR spectroscopy shows the dominant vibrational changes for $x \geq 0.6$. Zero field cooled/field cooled magnetization curves at $x = 0$ for CoCr_2O_4 showed paramagnetic to ferrimagnetic evolution at $T_C = 97$ K and spiral magnetic order at $T_S = 30$ K. T_C and T_S shows decreasing trend with increasing 'x' followed by an additional

AFM transition at $T_N = 15$ for $x = 0.6$. Dielectric properties improved when $x = 0.6$ in nanoparticles.

Galivarapu *et al.* [45] synthesized CoCr_2O_4 nanoparticles by coprecipitation method. Bulk CoCr_2O_4 undergoes a phase evolution from paramagnetic to ferrimagnetic state at spin spiral temperature (94 K) to a spiral order at T_S (~24 K), and in lock-in-transition under 15 K temperature. Reducing the size of CoCr_2O_4 to ~ 50 nm magnetic transition revealed that decreasing the size of nanoparticles, paramagnetic to ferrimagnetic transition is enhanced to 99 K, followed by a decrease in lock-in-transition (T_L) to 8 K.

Edrissi *et al.* [46] prepared pure CoCr_2O_4 nanoparticles through mixed chelates thermolysis of metals using 2-Merceptopyridine N oxide sodium salt as chelating agent. Prepared samples were characterized by using XRD, TEM thermogravimetric analysis and magnetic measurements of prepared sample have been done. The particle size was observed in the range of 4.1 nm as determined through XRD. It was found that temperature and time of thermolysis process has significant effect on the particle size reduction.

Akyol *et al.* [47] prepared CoCr_2O_4 nanoparticles by utilizing sol-gel synthesis technique and studied magnetic coupling with application of magnetic field. Crystal analysis show that particles are in cubic phase having particle size around 75 nm. SEM gives us information that particles are homogenously distributed in the sample. Magnetic measurements revealed that in CoCr_2O_4 nanoparticles paramagnetic to ferromagnetic and non-collinear spiral phase transition takes place at 96 and 27 K temperature. Magnetic transition are related to exchange bias effect which is observed to be decrease in exchange coupling at higher temperature. While the exchange coupling effect might be produced due to anisotropic exchange interaction between ferri and antiferromagnetic components. Samples has also shown shift in lock in transition state at 16 K for field heated magnetization curve and 8 K for field cooled curve of these nanoparticles.

Menyuk *et al.* [39] reported that in bulk CoCr_2O_4 , Ferrimagnetic and spin spiral state exist below T_C . Ferrimagnetic state shows long range order below T_C while spin spiral state exhibit short range order. Cone angle for ferrimagnetic long range order is calculated by using formula,

$$U = \frac{4SBJ_{BB}}{3SAJ_{AB}} \quad (2.1)$$

Here J_{BB} is the exchange integral between the spin of B-B site and J_{AB} is the exchange integral between the spin of A-B site. Where S_B and S_A are the magnitude of spins at Site A and Site B. J_{BB} interaction is much stronger than J_{AB} and also responsible for the magnetic properties in bulk CoCr_2O_4 .

Tian *et al.* [48] synthesized CoCr_2O_4 nanoparticles by using the hydrothermal technique. Size dependent magnetic properties were investigated. All prepared nanoparticle shows lower Curie temperature ($T_C \sim 87$ K) from paramagnetic to collinear short range ferrimagnetic state as compared to their bulk counterpart. By decreasing particle size, critical temperature also decreases and vanishes at approximately 2.8 nm due to spin disorder produced at the surface of nanoparticles. Nanoparticles with $D \leq 5.4$ nm cluster spin-glass appeared in CoCr_2O_4 nanoparticles. Glass transition temperature (T_g) was found at 16.3 K and decreases by decreasing the size of nanoparticles.

Chen *et al.* [49] examined the magnetic properties of CoCr_2O_4 nanoparticles and found that with decreasing temperature, CoCr_2O_4 nanoparticles went into ferrimagnetic transition at T_C then in long-range spiral transition at T_S and at last in lock-in transition state at T_L . Irreversible magnetizing behavior was shown by CoCr_2O_4 nanoparticles upon cooling the sample to 5K under 100 Oe. This magnetic behavior remains constant up to 45 KOe, which indicates co-existence of incommensurate and commensurate spiral orders in these nanoparticles. With applying pressure CoCr_2O_4 nanoparticles, T_S and T_L shows increasing trend indicating the enhancement in magnetic frustration due to lattice contraction.

Kamran *et al.* [50] investigated the magnetic properties of CoCr_2O_4 nanoparticles at different temperature ranges. ZFC/FC curves showed paramagnetic to ferrimagnetic transition at $T_C = 100$ K, spin spiral appeared at $T_S = 27$ K and finally lock-in transition takes place at $T_L = 13$ K. CoCr_2O_4 nanoparticles show negative magnetization under 50 Oe which get suppressed at higher fields. At higher fields T_C shifts toward higher temperature while T_S and T_L remains unchanged. M-H loops of these nanoparticles revealed ferrimagnetic trend at all temperature less than 100 K and almost paramagnetic at 100 K. An irregular decrease in M_s was found below to 5 K temperature which can be due to the presence of spin spiral and lock in state at lower temperature.

I. Sosnowska *et al.* [51] investigated the doping effect of Mn on Magnetic and structural properties of BiFeO_3 . Mn doping causes the structural changes in BiFeO_3 at microlevel observed through broadening in diffraction peaks. Broadening in peaks is referred due to anisotropic strain broadening. Mn doping changes the long range spiral magnetic order of BiFeO_3 to antiferromagnetic structure. Average magnetic moment was found to be decreasing with increasing concentration of Mn in the sample.

Pankaj Chaudhry *et al.* [52] synthesized the spinel chromite of $\text{Co}_{1-x}\text{M}_x\text{Cr}_2\text{O}_4$ ($M = \text{Zn, Mg, and Cu}$). XRD confirms the spinel structure of the sample. Structural changes are observed from cubic to tetragonal phase. Shifting of raman mode with additional raman active modes has been observed due to doping effect.

M. Younis *et al.* [53] synthesized MCr_2O_4 ($M = \text{Fe, Co, and Ni}$) by using sol-gel auto-combustion method. All the samples were calcined at 650°C . XRD confirmed cubic spinel structure of CoCr_2O_4 . Magnetic analysis of nanoparticle shows that CoCr_2O_4 show ferromagnetic behavior at 5 K temperature. Magnetic transitions were observed at different temperatures such as 80 K and 90 K respectively.

X. H. Chen *et al.* [54] investigated the magnetic properties of zinc chromite nanoparticles of various particle size distribution. Structural analysis was done by using XRD and TEM technique while SQUID was used for the magnetic measurement of nanoparticles. As the particle size of zinc chromite nanoparticle decreases, it tends to increase the magnetization of nanoparticles and also the antiferromagnetic transition

starts disappearing with decreasing particle size and also due to change in cationic distribution with in unit cell which further decreases the B-B site exchange interaction between lattice sites.

S. A. Gene *et al.* [55] investigated the structural and magnetic properties of spinel zinc chromite nanoparticles synthesized through thermal treatment method. Average crystallite size was found by using x-ray diffraction technique which was found to be 19 nm and starts increasing with increasing calcination temperature. Particle size was calculated by using transmission electron microscope which matched well with the earlier found crystallite size of nanoparticles. Magnetic properties was studied by using ESR which tells us about the existence of unpaired electrons and also decrease in resonant magnetic field (H_r) with the increase of calcination temperature shows an increase in magnetic properties of the sample.

Shandong Li *et al.* [56] prepared cobalt chromite nanoparticles under normal conditions. Shift in hysteresis loop was observed by applying external field and 627.9 kA/m coercivity was attained. XRD and HRTEM analysis tells us that lattice structure of cobalt chromite nanoparticles has been strongly distorted and surface defects were found in crystalline structure of nanoparticles. High value of coercivity is regarded because of lattice distortion.

K. Dwight *et al.* [57] investigated the magnetic properties of the $MnCr_2O_4$ nanoparticles by using neutron diffraction technique. Study shows that manganese chromite have shown deviation from spiral configuration while the magnetic moment of Mn^{++} is very less as compared to pure Mn. Magnetic moment of Mn^{++} was found to be $4.3 \mu_B$ while for pure Mn its value is $5 \mu_B$. Lower value of hyperfine field of Mn in observed in $MnCr_2O_4$ which is also attributed due to lower value of magnetic moment of Mn ion.

Chapter 3

Synthesis and Characterization Techniques

In nano materials, synthesis route are important to get the material in the nanoscale [58]. Synthesis route plays major role to obtain desired nanoparticles. Properties of material depends on the synthesis technique for the preparation of nanoparticle.

3.1 Synthesis techniques of nanoparticles

Two methods are being used for the synthesis of nanostructured materials.

1. Top down approach
2. Bottom up approach

3.1.1 Top down approach

In Top down approach bulk materials are broken down and we get small feature of nano molecule [59]. This method is not widely used because the particles formed in this method show structural defects also non-homogenous nanoparticles are obtained through this method. In this method different tools are used to cut and mold the materials to get into our required shape. Synthesis routes used in top down approach are:

- Ball Milling
- Lithography

3.1.2 Bottom up approach

Bottom up is a chemical approach used for the fabrication of nanoparticles. In this method, small atoms are joined together to form a large structure [59]. Nanoparticles obtained through this process are homogenous and show less structural defects. Also, nanoparticles obtained through this method show much stability as compared to obtained through top down approach which makes highly suitable to be used in different applications. Synthesis technique which are used in bottom up approach are:

- Sol-gel
- Co-precipitation

Fig 3.1 shows the top down and bottom up approach for the synthesis of nanoparticles.

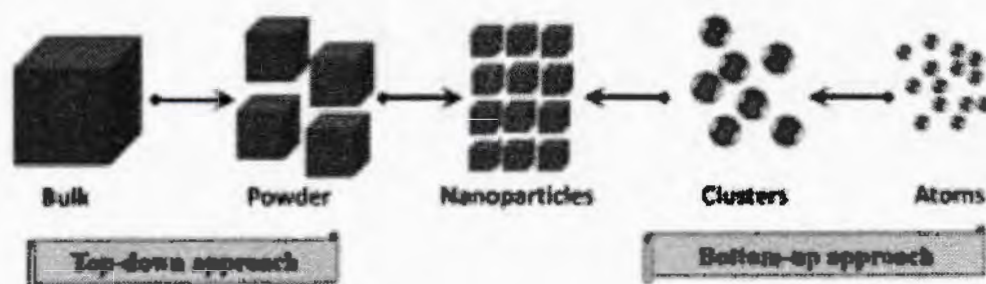


Fig. 3.1: Top down and bottom up synthesis approach for nanoparticles [60].

3.2 Synthesis of manganese doped cobalt chromite nanoparticles

Various synthesis techniques can be used for the preparation of samples but I have nominated sol-gel approach for the synthesis of $\text{Co}_{1-x}\text{Mn}_x\text{Cr}_2\text{O}_4$ nanoparticles.

3.2.1 Sol-Gel

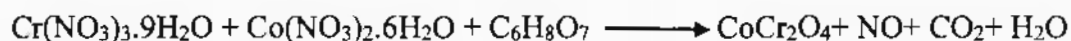
Sol-gel technique is used for the preparation of nanoparticles. By using this technique one can get nanomaterials from small atoms or particles. Sol-gel method includes advancement of inorganic systems to get the colloidal solution furthermore we use sol to get the gel keeping in constant fluid stage. In Sol-gel process, basic constituent of final products are used in well regulated reaction to form solid material. Structure and size of nanoparticles have strong dependence on reaction parameters and also on the properties of precursor materials. A sol is a steady suspension of colloidal particles (nanoparticles) in a fluid. While the particles can be amorphous or crystalline, and may have thick, permeable, or then again polymeric substructures. A gel comprises of a permeable, three-dimensionally consistent strong system encompassing and supporting a consistent fluid stage (wet gel). There are four important process that involves in sol-gel process, that are Hydrolysis, Condensation, Gellation and finally the drying process. In hydrolysis, bond breaking of precursor materials take place while in condensation small molecules join to form a large one. There are several parameter which affects the condensation process such as type of precursor used, catalyst, type of solvent, pH of the solution and concentration of the reactants used. pH of the solution also effect the other steps in sol-gel process such as minimum hydrolysis of solution takes place at $\text{pH} = 7$ while condensation at $\text{pH} = 4.5$.

In gellation, liquid solution dries up and formation of gel takes place due to evaporation of solvent from material. Finally in drying process, moisture from material evaporates and we get nanoparticles. But after the moisture being removed from gel several other things can happen such as the structural changes may produce in nanoparticles.

For Mn doped Cobalt chromite nanoparticles. Mn is added with different weight percentage in CoCr_2O_4 nanoparticles. Following chemicals were used for the synthesis of $\text{Co}_{1-x}\text{Mn}_x\text{Cr}_2\text{O}_4$ nanoparticles.

1. Cobalt Nitrate
2. Manganese Nitrate
3. Chromium Nitrate
4. Ethanol
5. Distilled Water
6. Citric Acid.

Chemical reaction that takes place for the synthesis of Cobalt chromite nanoparticles is as follows:



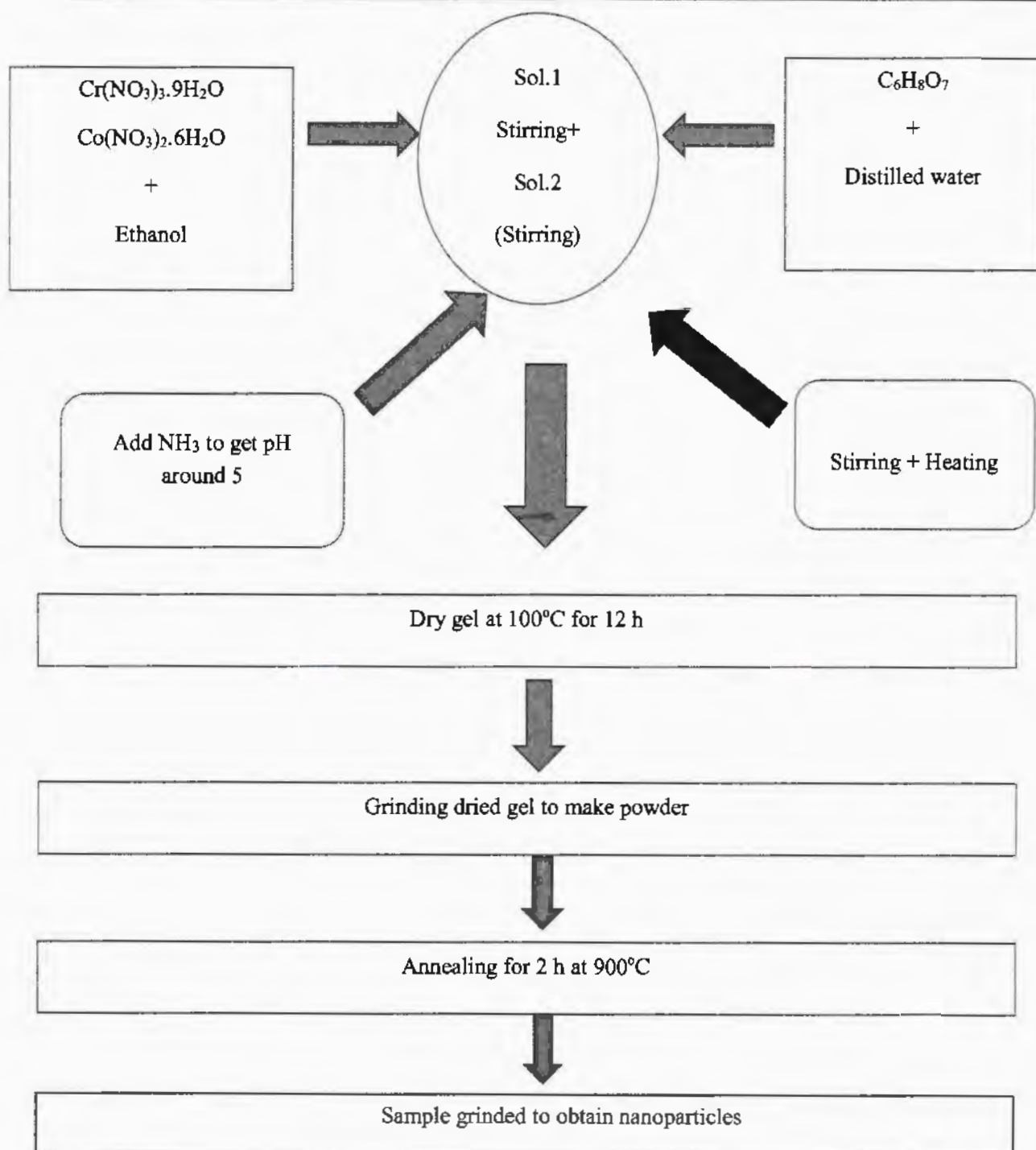
Synthesis of CoCr_2O_4 nanoparticles through Sol-gel method

Fig. 3.2: Flow chart for synthesis of cobalt chromite nanoparticles.

First of all I weighted the Chromium Nitrate $\text{Cr}(\text{NO}_3)_2 \cdot 9\text{H}_2\text{O}$ and Cobalt Nitrate $\text{Co}(\text{NO}_3)_2 \cdot 6\text{H}_2\text{O}$ in stoichiometric amount and dissolved them in ethanol in first beaker. Secondly, I took citric acid ($\text{C}_6\text{H}_8\text{O}_7 \cdot \text{H}_2\text{O}$) and distilled water in second beaker with molar ratio of 1 : 4 while citric acid was taken in molar ratio of 1 : 1 with nitrates. Then I have started stirring both the solutions to get well dispersed, uniform mixture. When $\text{C}_6\text{H}_8\text{O}_7 \cdot \text{H}_2\text{O}$ completely gets dissolved into the distilled water we added it dropwise into the first beaker pH of the solution was checked and kept around 5 to 6. I have added ammonia (NH_3) into the solution to maintain it's pH. After establishing the required pH value, the solution was heated upto 80°C . After heating the solution, a gel was formed. In order to remove mist from the gel, gel was placed in the oven for 12 h. The dried gel was grinded and then annealed at 900°C for 2 h in order to get desired Mn doped cobalt chromite nanoparticles [34]

3.3 Characterization techniques

Different type of characterizing tools can be used for the analysis of nanoparticles such as X-ray diffraction (XRD) used for the structural analysis of nanoparticles. TEM is used to examine the particle size, composition and shape. Vibrational properties of sample has been studied by using Fourier Transform Infrared Spectroscopy (FTIR). For Magnetic measurements, Superconducting quantum interference device (SQUID) magnetometer is used.

3.3.1 X-ray diffraction (XRD)

X-rays are highly energetic radiations. Energy of these rays is between 200 eV to 1 MeV. In electromagnetic spectrum these rays lie between gamma rays and ultraviolet (UV) radiations [61]. X-rays was first discovered by WC Roentgen in 1895 [62]. Wavelength of x-rays ranges from 0.5 \AA to 10 \AA . Longer wavelength of x-ray spectrum is known as soft x-rays ($0.5 - 1 \text{ \AA}$) while shorter wavelength of x-ray spectrum is referred as hard x-rays ($1 - 10 \text{ \AA}$). X-rays are non-destructive for crystal geometry and are being used to know about the crystal structure of solids, including lattice constant and geometry [63]. X-rays are produced in x-ray tube as shown in Fig. 3.3. There are four necessary condition for the production of x-rays: Production of electrons, Production of high speed electrons, Focusing electrons, stopping of high speed electrons.

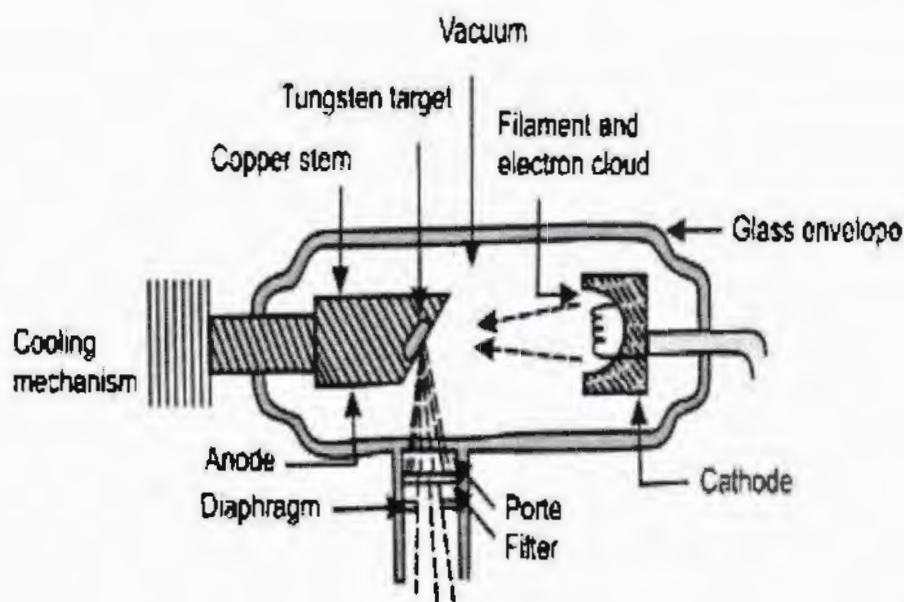


Fig. 3.3: X-ray tube [64].

Electrons are produced by hot filament made up of tungsten. Tungsten is used because it has high melting point. When the filament is heated, electrons start boiling off from the tip of hot filament. Electrons emitted from cathode filament are being accelerated to anode by a high voltage applied across the ends of x-ray tube. The higher will be the applied voltage, more speed will be gained by electrons. As electrons are being emitted by hot filament (cathode), all electrons have negative charge so they will repel each other and start spreading out, so a focusing cup is used around cathode whose electrical force causes the electrons to remain focused at one point. The point where electrons strike is called focal spot. Finally, electrons emitted from filament interact with the target and initially it produces heat, further it excites the electron present in the inner shell of an atom. This excitation and re-stabilization of electron produce lots of heat energy which generate x-rays. X-rays produced from target spread in all directions but only those escape out which are useful beam of x-ray energy. The process of inner shell transition in an atom by interaction of fast moving electron with the target material is shown in Fig.3.4 [65].

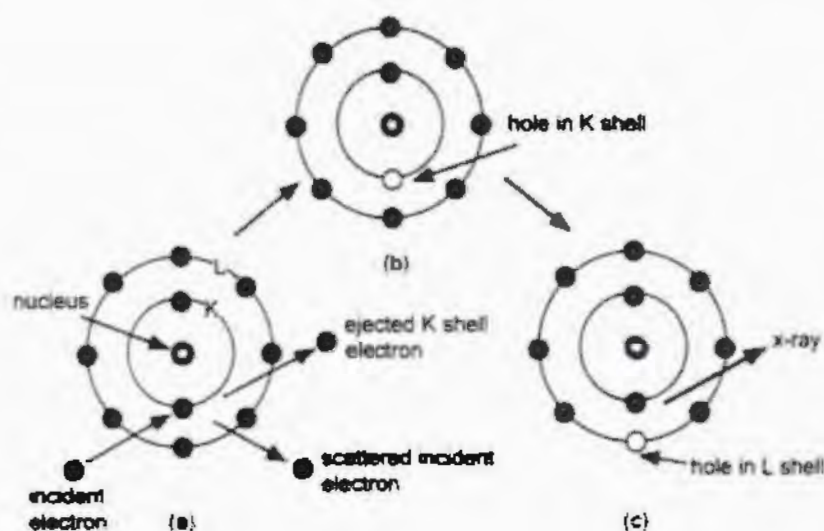


Fig. 3.4: Process of inner shell ionization a) incident electron ejects k shell electron from atom, b) left a hole in k shell and c) re-arrangement of electron takes place, cause emission of x-ray photon [61].

Fig. 3.5 shows the schematic diagram of x-ray diffraction Pattern. A material whose crystallographic information is required is placed between an x-ray source and a detector. When x-rays fall on a material. X-rays interact with crystal planes of a material and are diffracted by the crystalline part of the material while x-rays pass out straight from the amorphous part of crystal without being diffracted [63]. Diffracted rays move toward the detector where crystal pattern of material will form. It is to be noted that wavelength of x-rays fallen on a material should be comparable to that of the interatomic distance of atom. X-rays after being scattered from the crystal planes leaves the crystal by making angle 2θ with the crystal. Interference phenomena takes place between the diffracted x-rays from the material. Two type of interference can take place: constructive interference or destructive interference. Constructive interference takes place when rays are in phase after being diffracted while destructive interference take place when diffracted rays are out of phase to each other [66]. Constructive interference tell's us about the crystalline part of material while destructive interference shows the amorphous part of sample.

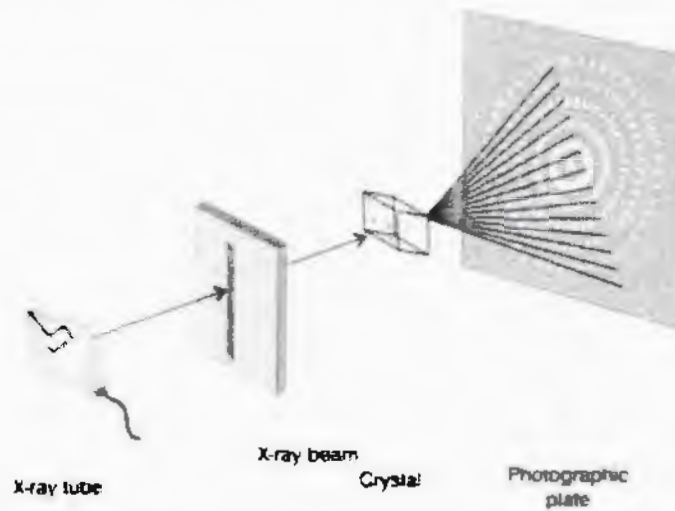


Fig. 3.5: Schematic diagram of x-ray diffraction pattern [66].

Bragg's law must be satisfied in order to get the constructive interference. Bragg's law states that the path difference between the two rays must be equal to an integral multiple of their wavelength as shown in Fig. 3.6. When the incident wave is equal to the path difference, they will superimpose, hence resulting in constructive interference [67]. Bragg's law was proposed by W. L. Bragg [68]. The mathematical relation used for Bragg's law is as follows,

$$n\lambda = 2d \sin \theta$$

(3.1)

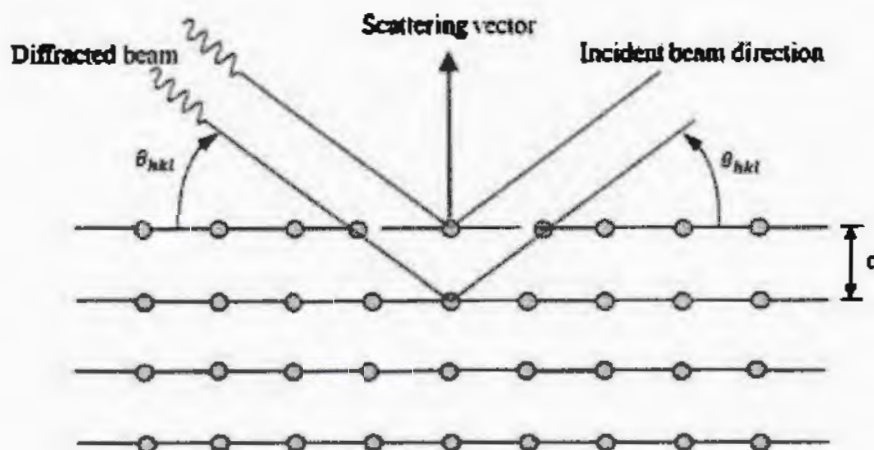


Fig. 3.6: Diagram of Bragg's law [69].

Where,

n = order of reflection

λ = wavelength of x-ray beam

d = distance between crystal planes,
of light

θ = angle between plane and beam

Average crystallite size (D) of nanoparticles can be estimated from the XRD pattern by using Scherrer's relation [1].

$$D = \frac{K\lambda}{\beta \cos \theta} \quad (3.2)$$

Where,

λ = X-ray wavelength,

β = full width at half maximum (FWHM)

K = Scherrer's constant

θ = diffraction angle.

3.3.2 Transmission electron microscopy (TEM)

TEM is commonly utilized for the structural analysis of nanoparticles which includes the lattice parameters, particle shape and crystallinity. Beside these capabilities of TEM, it can also be utilized to determine the melting point of crystals. Magnification power of TEM ranges from 50 to 10^6 .

Fig. 3.7 shows transmission electron microscope diagram. In Transmission Electron Microscopy, high energy beam of electron ranging from 100 KeV or higher up to 1 MeV are produced from electron gun. Electrons are ejected from electron gun in random direction, by means of condenser lenses electrons are focused onto the sample. Condenser lenses are actually electromagnetic lenses which works on the principle of Lorentz force. Sample is placed between condenser lens and objective lens. Electrons interact with the sample in two ways either deflected or undeflected depending upon the nature of sample. As electrons strikes the surface of the sample. Image of the sample forms which depends on the type of interaction between the sample and electron such as mass-thickness, phase and diffraction contrast. In mass-thickness contrast image will be darker due to large thickness of sample. While the image of the sample will be light. Intermediate lenses are

used to focus the diffraction pattern to be seen on fluorescent screen. Strength of intermediate lens can be changed for viewing the diffraction pattern clearly. The reason of high magnification of Transmission Electron Microscopy is due to small wavelength of electrons. The most important feature of TEM is that, we can obtain three dimensional crystal structure to examine the lattice parameters, space group and other information related to crystal [63].

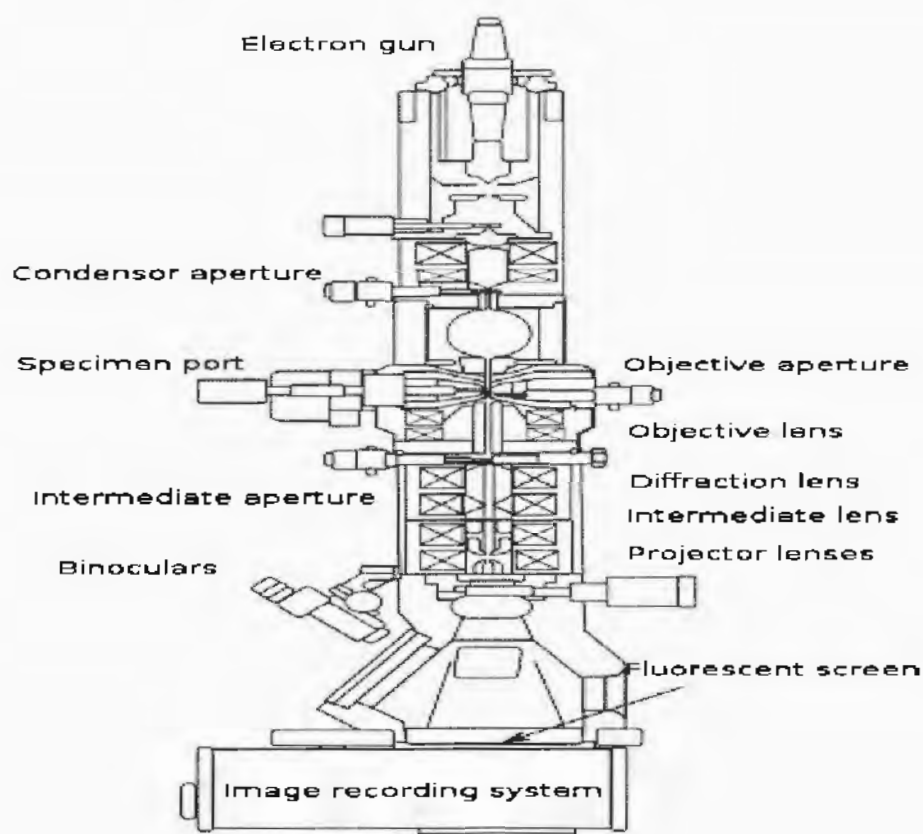


Fig. 3.7: Schematic diagram of transmission electron microscope [70]

3.3.3 Fourier transform infrared (FTIR) spectroscopy

Infrared spectroscopy is a technique used for the analysis of chemical compounds. Different chemical compounds or functional groups absorb IR radiations of different wavelength dependent upon the nature of functional group attached to a particular compound.

FTIR is an optical device used for elemental identification. It is also called as Interferometer. There are different type of interferometers but the most common type of interferometer used is called Michelson Interferometer as shown in Fig. 3.7. It was first

built in 1880s by Albert Abraham Michelson (1852-1931) and won noble prize on his discovery [71].

Michelson Interferometer has four arms. Top most arms consists of infrared source and collimating mirror to receive the light from IR source and make the rays parallel. The bottom arm contains a fixed mirror i.e, whose position cannot be changed while the right arm consist of moving mirror whose position can be changed. On the left arm, there is a sample and detector and the most important part of Interferometer is at the center of optical device called beam splitter. A beam splitter is designed in such a way that when light strike on its surface some portion of light transmit through it while some part of light is reflected back. Light transmitted through beam splitter move toward the fixed mirror while reflected light sent toward the moving mirror. After light being striked at moving and fixed mirror it recombines at beam splitter. After passing through beam splitter it interacts with sample and hit on the detector.

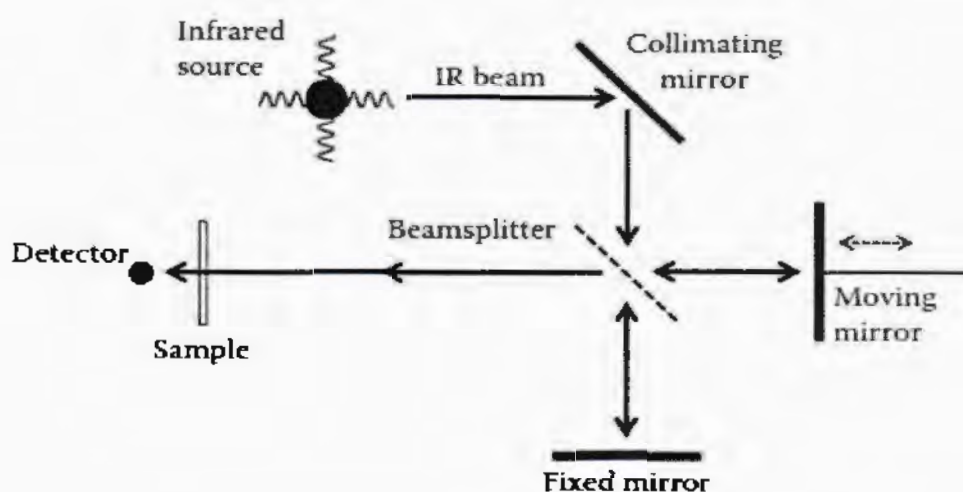


Fig. 3.8: Diagram of michelson interferometer [72].

After passing through beam splitter, the light interfere as follows,

$$A_f = A_1 + A_2 \quad (3.3)$$

A_f = Amplitude of Final light beam A_1 = Amplitude of beam from fixed mirror

A_2 = Amplitude of beam from moving mirror.

The two reflected beams can undergo constructive or destructive interference. A_f will be greater than A_1 and A_2 if constructive interference take place while A_f will be less than A_1 and A_2 if destructive interference will occur between two light beams. The condition for the two light beams to combine constructively after reflection from mirrors is that the path difference between the two light beams is integer multiple of their wavelength shown in Fig. 3.9.

$$\delta = n \lambda \quad (3.4)$$

Where, δ = Optical path difference,

λ = Wavelength

$n = 0, 1, 2, 3 \dots$ (any integer)

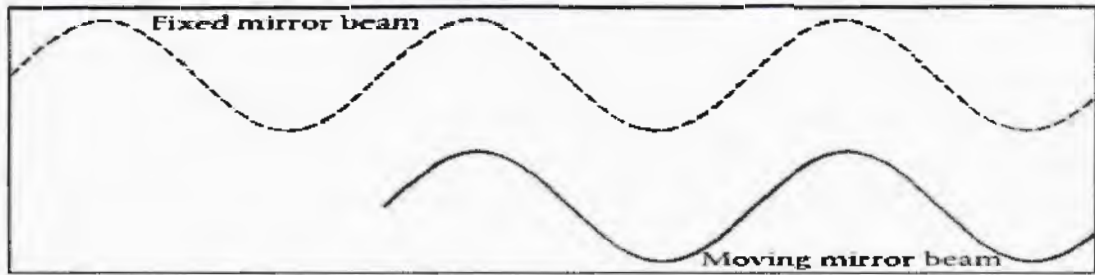


Fig. 3.9: Constructive interference of two light beams [72].

For the destructive interference to take place, optical path difference between the two light waves is equal to integer number of cycles plus half a cycle out of phase with each other as shown in Fig. 3.10. Mathematical form for destructive interference is,

$$\delta = (n + \frac{1}{2}) \lambda \quad (3.5)$$

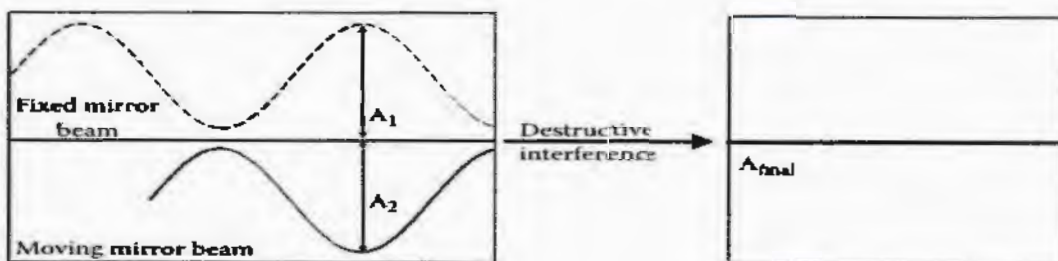


Fig. 3.10: Destructive interference shown by light waves [72].

FTIR gives us information about light intensity and wavenumber. Fourier transform tells us light of which wavenumber is present in a source. Amplitude of the Fourier spectrum tells us amount of light hitting the detector in terms of wavenumber.

3.3.4 Superconducting quantum interface device (SQUID)

magnetometer

Squid Magnetometer works by using phenomena of flux quantization and Josephson tunneling [73]. It is used to measure the magnetic field produced by the various materials. Squid is very sensitive device which can measure magnetic field from very small scale 10^{-15} T to a maximum value of 7 T [74]. Squid was first commercially made available in 1970. It was so sensitively configured that it can detect very small magnetic field such as Earth's magnetic field, even the magnetic field generated by Human heart and brain can be easily detected by using SQUID magnetometer. SQUID works in the temperature range of 4.2 K to 400 K. Josephson junction is an important part of Squid which was invented by Brian Josephson in 1962. Josephson effect takes place in Josephson junction which is the flow of current over a long period of time without applying any external voltage. Two superconductors are used in Josephson junction which are separated by a faint layer of some non-conducting material shown in Fig. 3.11. Quantum tunneling takes place when two electrons pass through insulating material under externally applied magnetic field. Tunneling of electrons produced circulating current in a junction. This phenomena is known as Josephson effect [75].

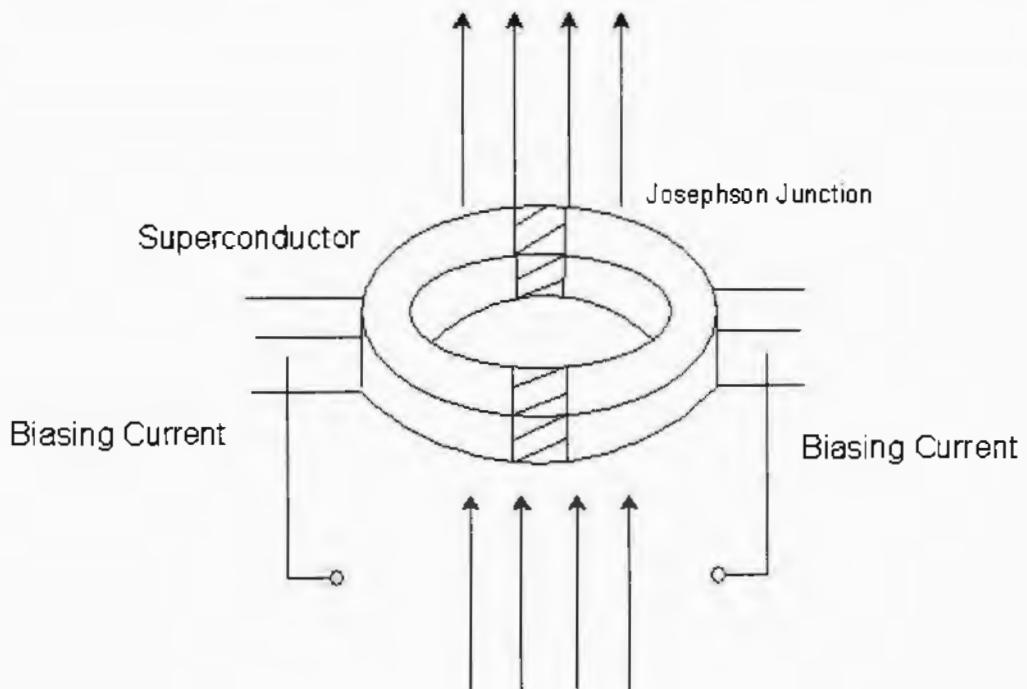


Fig 3.11: Schematic diagram of SQUID [76].

Squid has superconducting closed loop and current flow in it while superconducting loop can have one or more Josephson junction. Squid is considered to be the most sensitive device for measuring the magnetic properties of a material but it cannot directly measure the magnetic field produced by sample. Sample is moved up and down by superconducting coils which produces change of flux in the sample shown in Fig. 3.12. Due to change of flux, change in persistent current is detected. Which is further connected to Squid by using superconducting wires. Squid then convert the current into the output voltage [77]. Squid works as current to voltage converter, a very slight change in the current produced in the detection coils results in the change of output squid voltage which finally produces change in the magnetic moment of the sample.

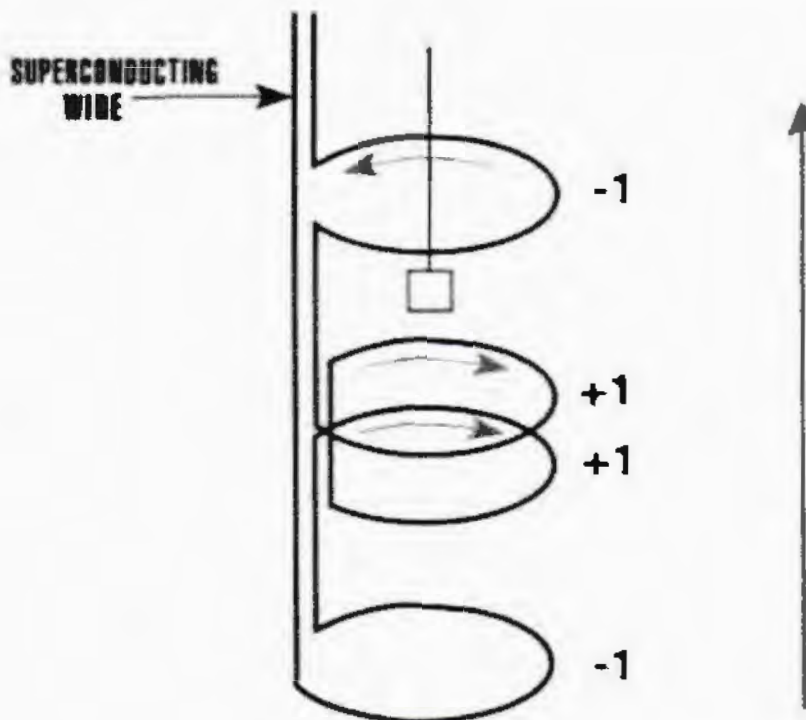


Fig. 3.12: Superconducting coil in SQUID [78].

Squid being too much sensitive to changes produced in external magnetic field, it must be shielded from the magnetic field produced in the surrounding atmosphere of laboratory and also from the magnetic field produced by large superconducting magnets. So the required magnetic field shielding is provided by the superconducting shield. This shielding effect do not make the magnetic field inside the squid to zero, but it makes a small and constant level of magnetic field which makes the squid to work without any interference from external magnetic field. For a squid to work properly, it does not required zero magnetic field inside it but a constant and small level of magnetic field. So the major purpose that are served by superconducting shield are:

- To maintain the ambient magnetic field produced in the laboratory.
- To protect the squid detector from the magnetic field produced by the superconducting magnet.

Detection coil used in squid magnetometer are superconducting wires wound in a set of three coils. The upper coil being wound in clockwise direction while there are two turns of the centre coil in the anticlockwise direction and finally the bottom coil is consistent in

direction with top coil having clockwise direction. After the detection coils being installed in MPMS as shown in Fig. 3.13 they are placed at the middle of the superconducting magnet so that magnetic field generated by the sample interact with the detection coils.

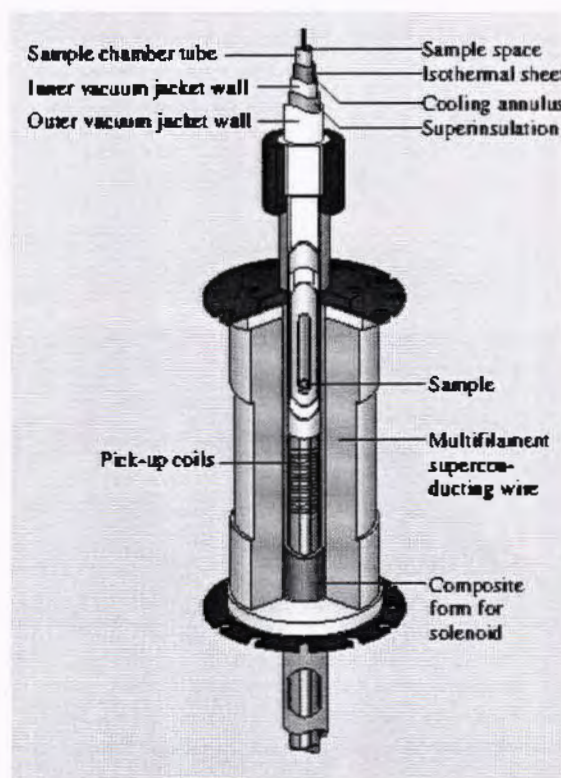


Fig.3.13: MPMS Squid [79]

The arrangement of detection coil is so adjusted that if the magnetic field in squid is settling down uniformly then the magnetic field generated by the top and bottom coil will be exactly cancelled by the coil being at the middle position. Another important point is that, if there is a small difference in the area of wound wires with respect to one another, it will create an imbalance between the coils and causes the system to become more sensitive to the ambient magnetic fields. In squid, superconducting magnets are arranged in superconducting loop. Magnets are allowed to charge upto to specific level so that they work in persistent mode, without the support of any other or external source of energy. Finally to measure the sample's magnetic moment, sample is placed on sample holder and made to enter into the superconducting loop, which move the sample up and down in the detection coils, changing the magnetic field and hence the magnetic flux through the sample. During the sampling process, sample is stopped at different places in detection

coils to take several squid output voltage which will measure the magnetic moment of the sample.

Chapter 4

Results and Discussion

4.1 Introduction

Multiferroics are material that possess both ferroelectric and ferromagnetic ordering at the same temperature. In these type of materials, electric field takes control of magnetic dipoles while magnetic field took control of electric dipoles [80, 81]. Co-existence of these two states has gained much more attention in scientific research society. Due to their unique physical and chemical properties, these materials are favourable for applications such as data storage, transformer cores, spintronic and humidity sensors [35, 45, 82]. Multiferroic cobalt chromite (CoCr_2O_4) nanoparticles belongs to spinel family which exhibits the ferroelectric and ferromagnetic coupling [49, 83]. General formula used for spinel compound is AB_2O_4 where A is a divalent cation which occupies the tetrahedral lattice site while B is trivalent cation located at octahedral lattice sites of a crystal respectively [34]. In CoCr_2O_4 nanoparticle unit cell, there are 32 oxygen ions, 64 tetrahedral lattice sites are available out of which 8 are filled while 16 octahedral lattice sites are filled out of 32. These nanoparticles contain ferrimagnetic nature [35]. Different type of exchange interactions take place between A (tetrahedral) and B (octahedral) lattice sites of these nanoparticles such as J_{AA} , J_{AB} and J_{BB} . J_{BB} interaction is strongest among all other interactions which controls the magnetic properties of CoCr_2O_4 nanoparticles [84]. There are also three phase transitions in CoCr_2O_4 nanoparticles which occurs at different temperatures that includes paramagnetic to ferrimagnetic phase transformation at Critical temperature (T_C), long range spiral order at (T_S) and lock-in transition state at (T_L). Dutta *et al.* [84] observed two magnetic transitions in sonochemically synthesized CoCr_2O_4 nanoparticles at $T_C = 84$ K and $T_S \sim 22$ K but bulk CoCr_2O_4 exhibit these two at $T_C = 98$ K and $T_S \sim 26$ K. Decrease in T_C and T_S is attributed to finite size effect. Chandana *et al.* [37] reported that CoCr_2O_4 nanoparticle prepared by co-precipitation method shows paramagnetic state to superparamagnetic state while bulk shows paramagnetic to long range order ferrimagnetic state at Curie temperature (T_C). T_C and T_S remains the same as the particle size reduced from bulk to nanoscale range. Kamran *et al.* [34] studied the structural and magnetic properties of multiferroic $\text{Co}_{1-x}\text{Mg}_x\text{Cr}_2\text{O}_4$ nanoparticles. ZFC/FC magnetization curves at $x = 0$ for CoCr_2O_4 showed paramagnetic to

ferrimagnetic transition at $T_C = 97$ K and spiral magnetic order at $T_S = 30$ K. T_C and T_S shows decreasing trend with increasing x followed by an additional AFM transition at $T_N = 15$ for $x = 0.6$. At $x = 1$, system changes into highly frustrated AFM structure due to formation of pure $MgCr_2O_4$.

Afzal *et al.* [85] prepared Cr_2O_3 and $MnCr_2O_4$ by chemically driven sol-gel synthesis route. Magnetic properties of sample were investigated by varying the external magnetic field and temperature. Cr_2O_3 has shown paramagnetic behavior at 300 K temperature and also at 5 K. In $MnCr_2O_4$ nanoparticles, paramagnetic to ferromagnetic phase transition takes place at $T_C \sim 50$ K. Zhou *et al.* [86] examined the magnetic properties of $MnCr_2O_4$ while focusing on the spin spiral transition around T_S . It was noticed that magnetic behaviour around T_S inhibits at higher magnetic fields. Externally applied magnetic field upto 5 T has not affected the spin spiral state as observed by specific heat measurement. Upon the application of external pressure at 5 K, coercivity increases which suggest us the increasing strength of spin spiral state. It was found that as we decrease the temperature at T_S spiral component develops perpendicular to the direction of parent ferrimagnetic state and it has not facilitated in increasing the saturation magnetization of the material.

Mn doping effect on magnetic properties of $CoCr_2O_4$ nanoparticles has not been investigated extensively so, we have doped Manganese (Mn) into $CoCr_2O_4$ nanoparticles. Our primary focus is to check the doping effect of Mn on magnetic phase transition temperatures such as T_C , T_S and T_L . Mn is a basically paramagnetic material with unfilled 'd' orbital which follow John Teller effect which will cause geometric distortion in $CoCr_2O_4$ crystal structure. Also, Magnetic moment of Mn is large ($5 \mu_B$) as compared to cobalt ($3 \mu_B$) [87] so it will tend to increase the saturation magnetization of $CoCr_2O_4$. Aakash *et al.* [88] synthesized Mn doped Nickel ferrite nanoparticles by co-precipitation technique. XRD data shown an increase in lattice constant with the increasing concentration of Mn in the sample due to large ionic radii of Mn (0.83 \AA) as compared to Ni (0.79 \AA). Williamson - Hall plot revealed the strain effect produced in crystallographic structure of $NiFe_2O_4$ nanoparticles due to large ionic radii of Mn. Magnetization studies shows that sample possess very low magnetocrystalline anisotropy coupled with ferrimagnetic nature.

In this research thesis, we will study the doping effect of Mn on structural, vibrational and magnetic properties of $CoCr_2O_4$ nanoparticles. XRD technique is used for structural analysis, TEM is used to study the morphology, FTIR is used for the

vibrational analysis and SQUID magnetometer is used to measure the magnetic properties of Mn doped CoCr_2O_4 nanoparticles.

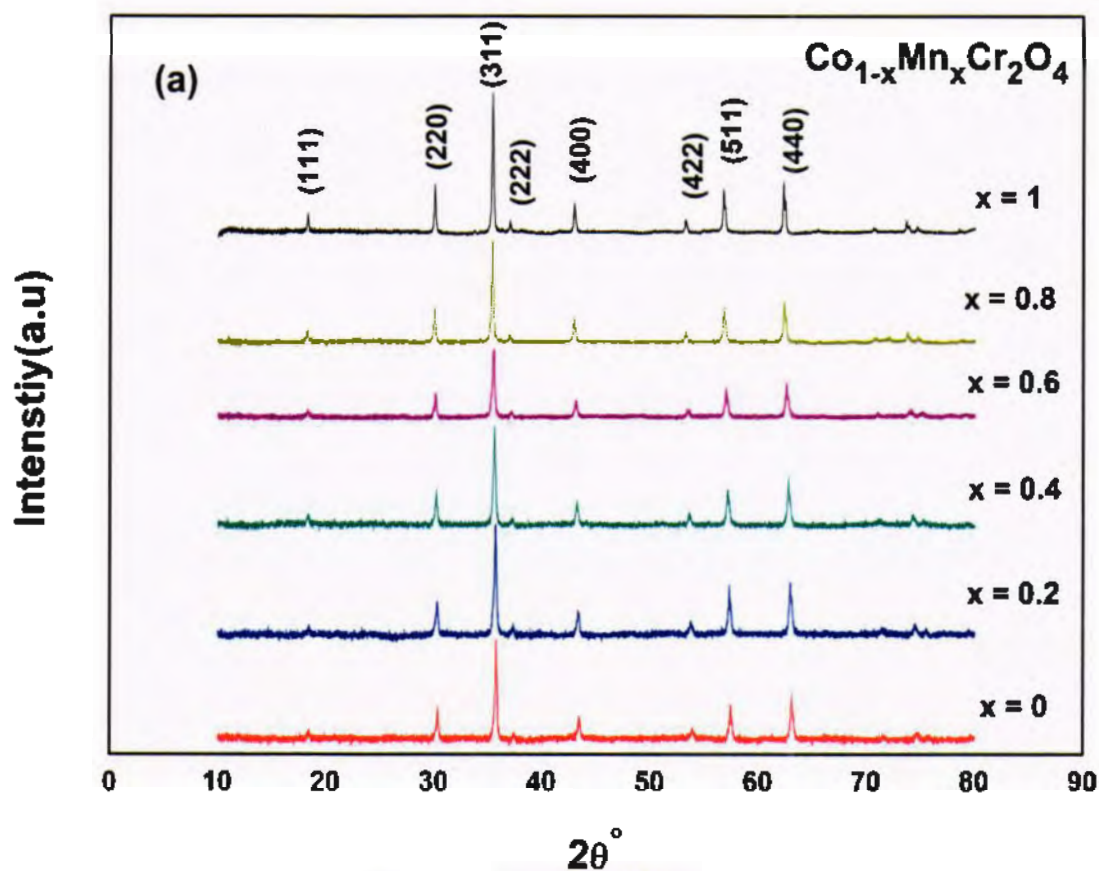
4.2 X-ray diffraction

We have done X-Ray Diffraction (XRD) for the structural analysis of the nanoparticles. Fig. 4.1 (a) depicts the XRD pattern of $\text{Co}_{1-x}\text{Mn}_x\text{Cr}_2\text{O}_4$ nanoparticles where $x = 0.0, 0.2, 0.4, 0.6, 0.8$ and 1 nanoparticles. For CoCr_2O_4 and MnCr_2O_4 nanoparticles, major diffraction peaks are obtained at $2\theta = 18.1^\circ, 30.3^\circ, 35.7^\circ, 43.4^\circ, 53.9^\circ, 57.4^\circ, 63.1^\circ$ belong to (111), (220), (311), (400), (422), (511) and (440) crystal planes, respectively which confirms the formation of cubic spinel structure of CoCr_2O_4 and MnCr_2O_4 nanoparticles. Peaks obtained in XRD pattern match well with earlier reported peaks for both types of nanoparticles [86, 89]. There is no extra peak for impurity constituent in it which confirm the single phase formation of our nanoparticles. There is also no change observed in cubic spinel structure with doping of Mn at Co in CoCr_2O_4 nanoparticles while peak intensity goes on increasing with the increasing concentration of Mn in CoCr_2O_4 nanoparticles. Mn being a transition metal, when it is doped in CoCr_2O_4 nanoparticles it introduces jahn teller effect which cause geometrical distortion. Thus, lowering the symmetry from cubic to tetragonal structure through compression of tetrahedral lattice sites [90]. But macroscopically crystal structure remains cubic due to short range ordering which cannot be easily detected by X-rays [88]. Due to bond compression, diffraction peaks start shifting toward lower value of 2θ indicating strain induced in crystal structure due to doping of larger ion (Mn) to smaller ion (Co). Average crystallite size (D) was calculated from XRD data by using Debye- Scherrer's formula that is given as:

$$D = \frac{K\lambda}{\beta \cos \theta} \dots \dots \dots (4.1)$$

Where, ' λ ' is X-ray wavelength (0.1541 nm), ' β ' is Full width at half maximum (FWHM), ' θ ' is diffraction angle and 'K' is shape constant and its value is 0.91 for spherical shaped particles. Fig. 4.1(b) depicts the average crystallite size of $\text{Co}_{1-x}\text{Mn}_x\text{Cr}_2\text{O}_4$ nanoparticles with different concentration of Mn. Average crystallite size was found in the range of 36 to and 47 nm. Average crystallite size shows minimum value for At $x = 0.2$ concentration. With further increase of Mn concentration in sample, increasing trend of crystallite size is observed. This can be attributed due to

change in cationic distribution of ions. With increasing concentration of Mn, it causes the migration of Co from tetrahedral site to octahedral site. At octahedral site, there is large bond length and also lattice expansion takes place due to replacement of smaller Co^{2+} ion (0.74 Å) [87] by larger Mn^{2+} ion (0.83 Å) [88] which causes an increase in crystallite size of nanoparticles.



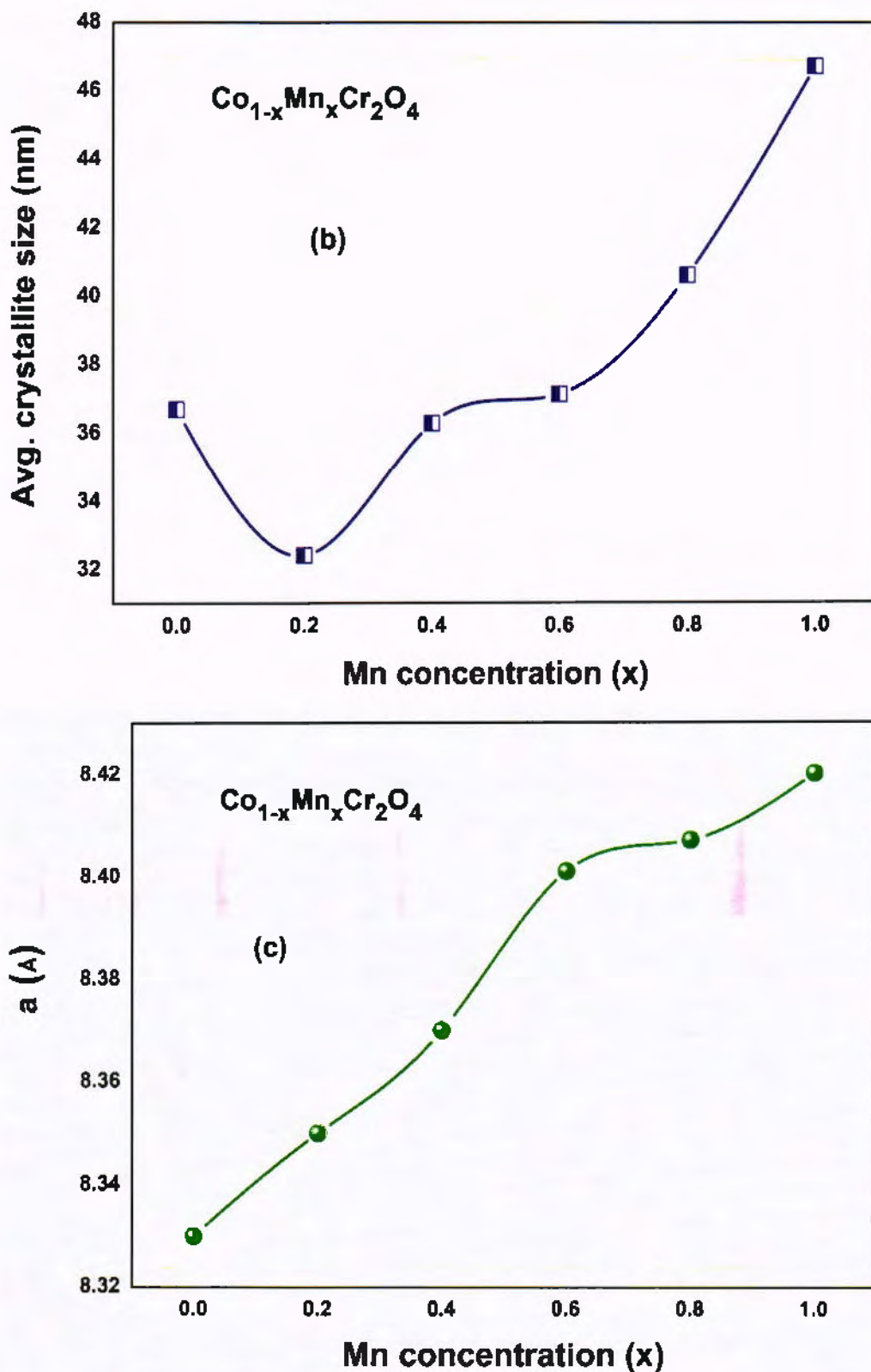


Fig. 4.1: (a) XRD patterns of $\text{Co}_{1-x}\text{Mn}_x\text{Cr}_2\text{O}_4$ nanoparticles (b) variation of average crystallite size and (c) lattice constant with Mn concentration (x). In (b) and (c), line just shows the trend.

Lattice parameters of these nanoparticles are also calculated by using the formula,

$$a = d \sqrt{h^2 + k^2 + l^2} \dots\dots\dots(4.2)$$

Where h, k, l are miller indices of crystal plane, 'a' is the lattice constant of simple cube and 'd' is the inter planer spacing. Fig. 4.1(c) shows the average crystallite size of $\text{Co}_{1-x}\text{Mn}_x\text{Cr}_2\text{O}_4$ nanoparticles with different concentration of Mn. Lattice parameters also reveal increasing trend with the increase of Mn concentration in CoCr_2O_4 nanoparticles. The lattice constant was found in the range of 8.33 Å to 8.42 Å and maximum was for MnCr_2O_4 nanoparticles. This effect is also attributed to replacement of small ionic radii Co by large ionic radii Mn. These results show good agreement with literature [39].

4.3 Transmission electron microscopy

Transmission Electron Microscopy (TEM) is used to study the morphology of nanoparticles. Fig 4.2 revealed the TEM images of MnCr_2O_4 nanoparticles at 50 nm and 200 nm scale. The images reveal cubic like shape and agglomerated nanoparticles with broad particle size distribution.

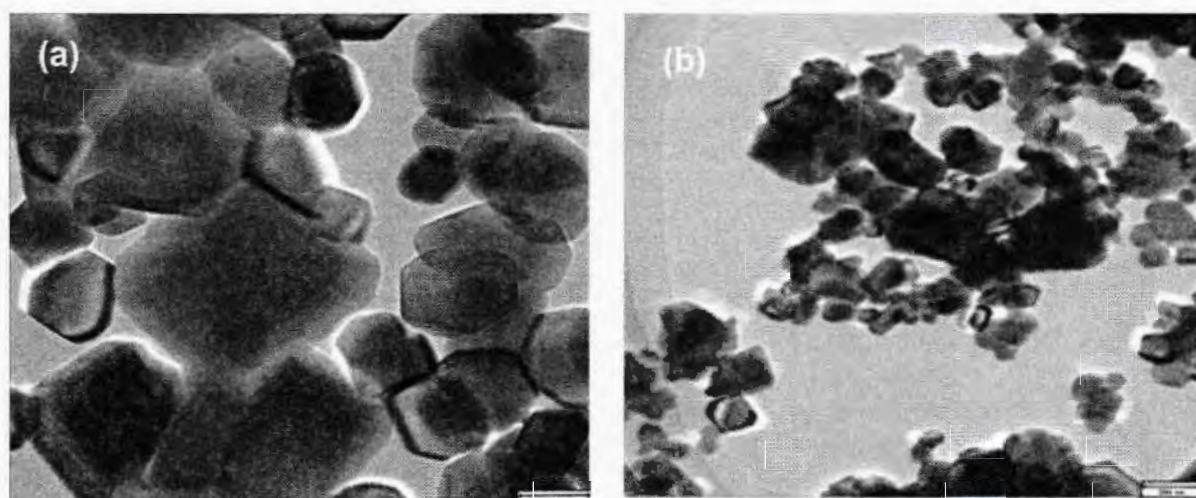


Fig. 4.2: TEM Images of $\text{Co}_{1-x}\text{Mn}_x\text{Cr}_2\text{O}_4$ nanoparticles at (a) 50 nm and (b) 200 nm scale.

4.4 Fourier transform infrared spectroscopy

Fig. 4.3 shows Fourier transform infrared spectroscopy (FTIR) spectra of Mn doped CoCr_2O_4 nanoparticles. FTIR reveals tetrahedral and octahedral vibrational bands lie in the range of 642 cm^{-1} to 609 cm^{-1} and 521 cm^{-1} to 482 cm^{-1} , respectively. Wide transmission bands are observed in CoCr_2O_4 nanoparticles and this broadness decreased with increasing concentration of Mn which is attributed to change in cationic distribution of nanoparticles [91]. Additional band is observed at 985 cm^{-1} which is overcome by the doping of Mn in the sample.

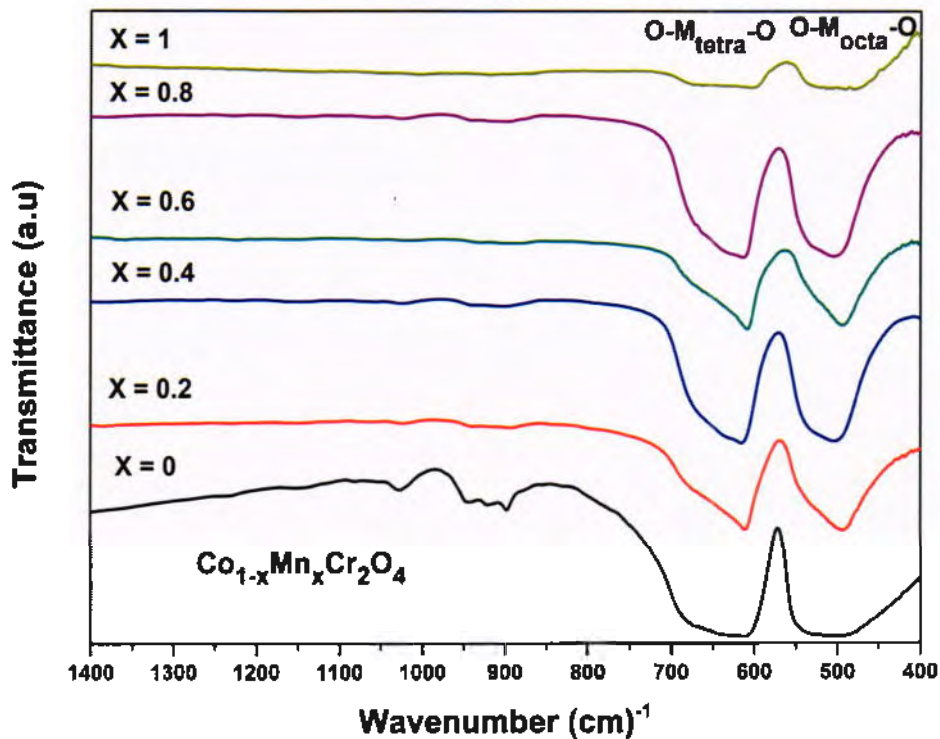


Fig. 4.3: FTIR spectra of $\text{Co}_{1-x}\text{Mn}_x\text{Cr}_2\text{O}_4$ nanoparticles.

4.5 Magnetic properties

To investigate the magnetic properties of Mn doped CoCr_2O_4 nanoparticles, Superconducting quantum interface device (SQUID) magnetometer is used. ZFC/FC curves and M-H loops are taken for the analysis of magnetic properties of these nanoparticles.

4.5.1 Zero field and field cooled magnetizations

Temperature dependent magnetic properties of Mn doped CoCr_2O_4 nanoparticles are studied by using ZFC/FC curves. Fig. 4.4 depicts ZFC/FC curves of Mn doped Cobalt chromite nanoparticles at 50 Oe field. Being multiferroic material, CoCr_2O_4 nanoparticles has shown different phase transitions: paramagnetic to ferrimagnetic state at 100 K, short range conical spin spiral state at 30 K and lock-in transition state at 10 K. It behaves paramagnetic material above 100 K. Increase in magnetization below spiral state, suggest the superparamagnetic behavior of CoCr_2O_4 nanoparticles as explained by Rath *et al* [37]. The temperature dependent magnetic transitions produced by CoCr_2O_4 nanoparticles are very near to prepared by Kamran *et al* [50]. The negative magnetization is observed at $x = 0$ and $x = 0.2$ Mn concentration which is attributed to the presence of uncompensated spins at grain boundaries of nanoparticles [92] and/or trapped small magnetic field in sample space

and coil of magnetometer during cooling process [93]. Increase of Mn concentration in CoCr_2O_4 nanoparticles, causes shifting of T_C towards the lower temperature 100 to 54 K along with suppression of T_S and T_L . This change is attributed to transformation of structure from a low frustrated magnetic structure to highly frustrated magnetic structure. Mn doping not only effect on temperature dependent magnetic transitions but also effects the magnetization of CoCr_2O_4 nanoparticles. Increasing concentration of Mn increases magnetization of FC curves because of the alignment of magnetic moments in the externally applied magnetic field of 50 Oe. On the other hand, T_C of MnCr_2O_4 is found to be 54 K. It also shows magnetic transition from FiM to AFM at Neel temperature (T_N) 20 K. AFM behavior of Mn is due to the fact that Mn being a transition metal it changes its oxidation state from Mn^{2+} to Mn^{3+} to balance the net charge of unit cell that was created due to change in cationic distribution of unit cell. Change in oxidation state takes place at low temperature. As a result, a change of its magnetic moment occurred from $5 \mu_B$ (Mn^{2+}) to $3 \mu_B$ (Mn^{3+}) which is equivalent to magnetic moment of Cr^{3+} ($3 \mu_B$). Hence MnCr_2O_4 show antiferromagnetic behavior at low temperature [94]. MnCr_2O_4 also has a large lattice constant as compared to CoCr_2O_4 that's why it shows less magnetic frustration and long range ferrimagnetic state [86].

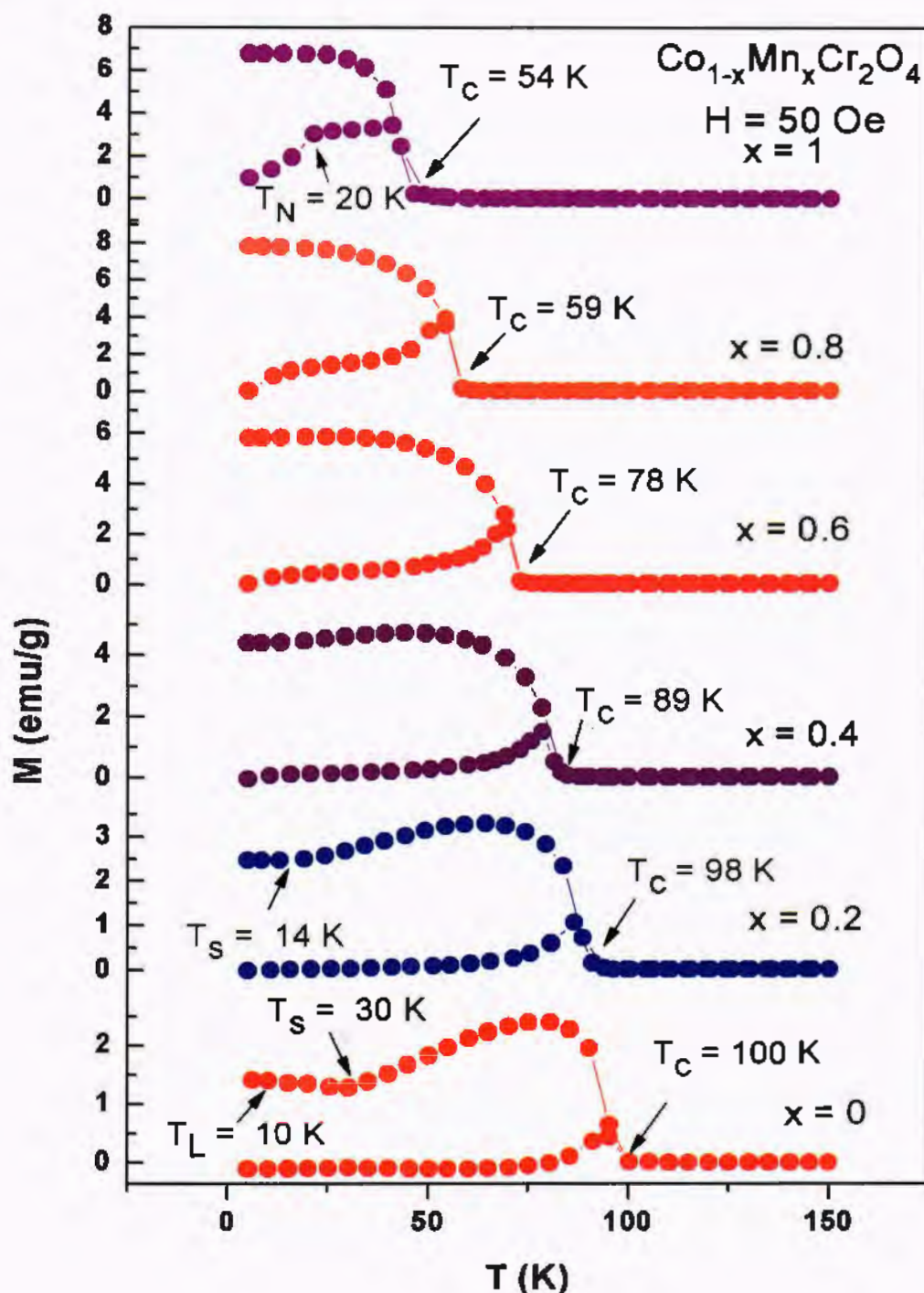
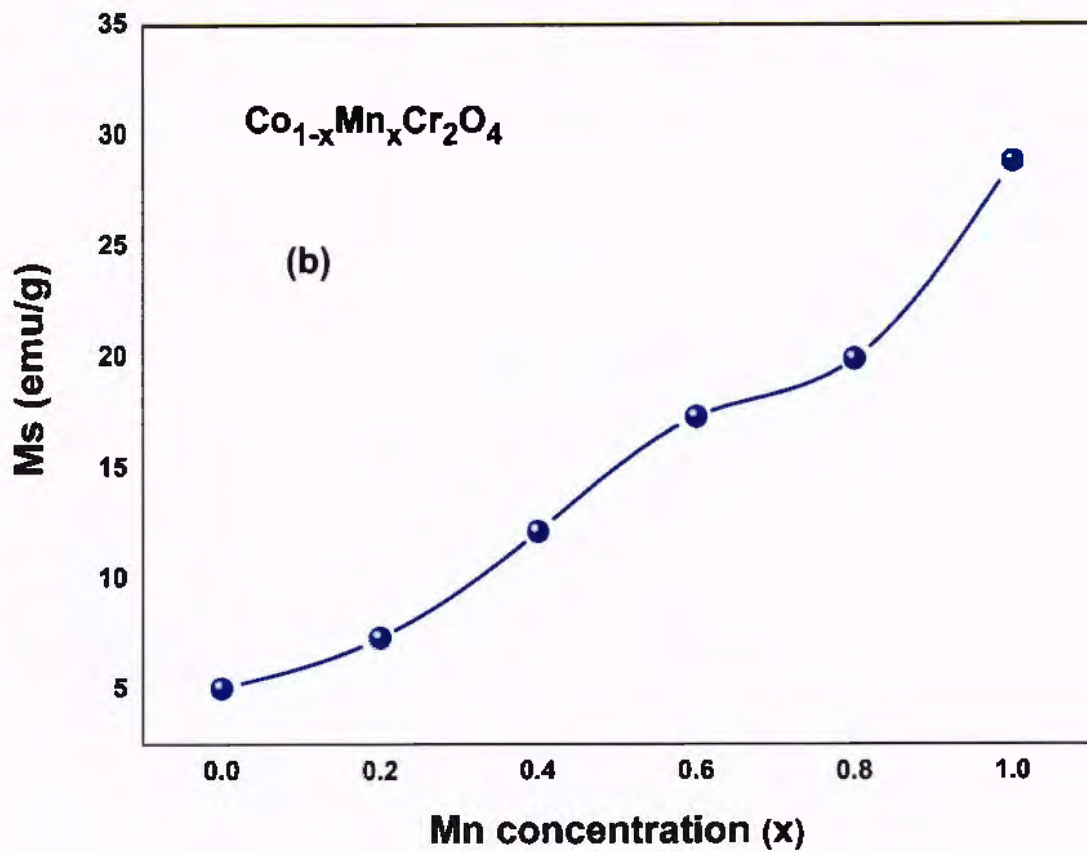
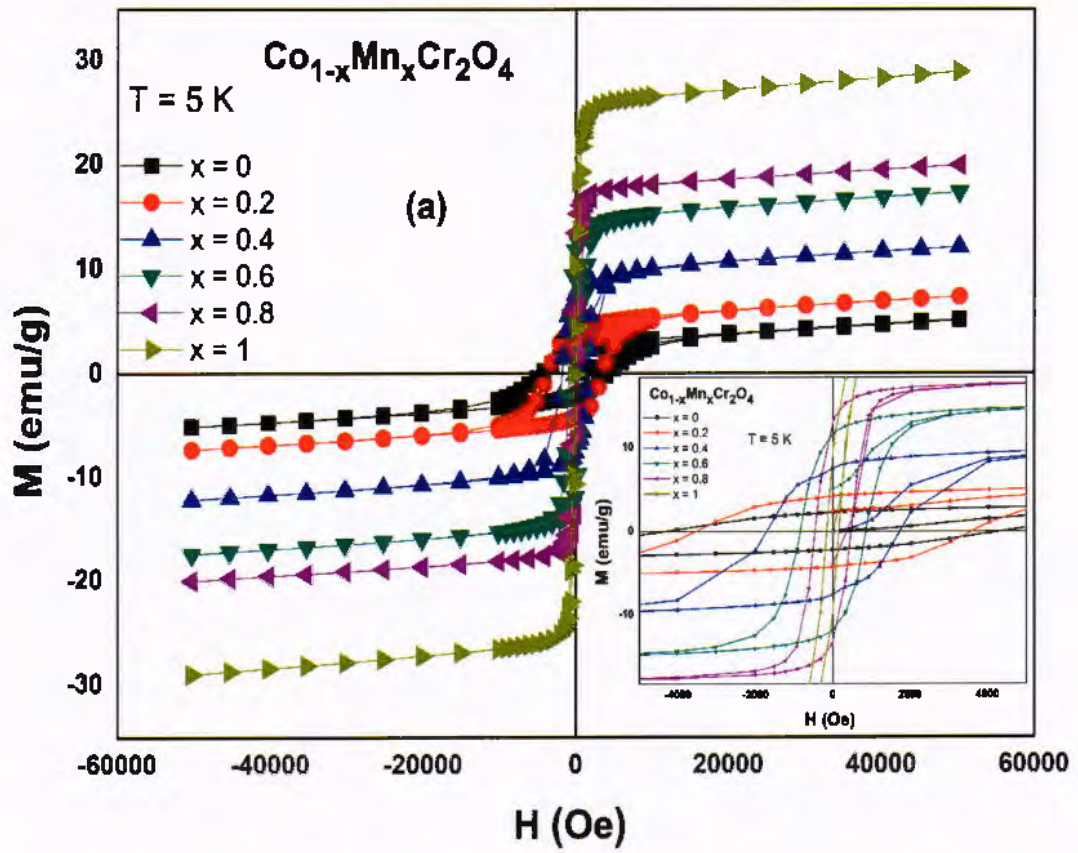


Fig. 4.4: ZFC/FC Curves of $\text{Co}_{1-x}\text{Mn}_x\text{Cr}_2\text{O}_4$ nanoparticles under $H = 50$ Oe field.

4.5.2 M-H loops

Fig. 4.5 (a) depicts the M-H loops of Mn doped CoCr_2O_4 nanoparticles at 5 K temperature and inset of Fig. 4.5 (a) shows the zoomed coercivity region. Due to random surface spins these loops are not saturated even at higher field. All the loops show typical ferrimagnetic behaviour which are good agreement with our ZFC/FC results. CoCr_2O_4 nanoparticles shows similar trend like hard magnetic materials

having large hysteresis loop area. The observed value of saturation magnetization and coercivity of CoCr_2O_4 nanoparticles is 5.05 emu/g and 4.4 kOe, respectively. Fig. 4.5 (b) display the variation of saturation magnetization (M_s) of CoCr_2O_4 nanoparticles with different concentration of Mn. As we increase the Mn concentration in the nanoparticles, M_s also starts increasing and the maximum value of M_s is found for MnCr_2O_4 nanoparticles. The value of M_s for all concentration of Mn $x = 0.2, 0.4, 0.6, 0.8$ and at 1 are 7.35, 12.15, 17.32, 19.92 and 28.82 emu/g, respectively. Fig. 4.5 (c) shows variation of coercivity (H_c) of CoCr_2O_4 nanoparticles with different concentration of Mn. The value of coercive field shows decreasing trend with increasing concentration of Mn. The maximum value of H_c is found for CoCr_2O_4 nanoparticles. The value of H_c for all concentration of Mn $x = 0.2, 0.4, 0.6, 0.8$ and at 1 are 3.5, 1.7, 0.97, 0.47 and 0.16 kOe, respectively. Increasing concentration of Mn suggests that all crystallites in material have the same direction, which causes increase in magnetization and lower value of coercivity. Mn belongs to soft magnetic materials. Magnetic moment of Mn is $5 \mu_B$ and of Co is $3 \mu_B$ due to which magnetization increases with the increasing concentration of Mn in CoCr_2O_4 nanoparticles. It also affects the coercivity and remanent magnetization of nanoparticles [87]. Coercivity of nanoparticles is related to magnetocrystalline anisotropy characteristic. CoCr_2O_4 nanoparticles have high value of magnetocrystalline anisotropy as compared to Mn that's why it shows high value of coercivity but as Mn concentration increases in sample coercive field start decreasing. This dramatic decrease in H_c suggest that sample show superparamagnetic like behaviour.



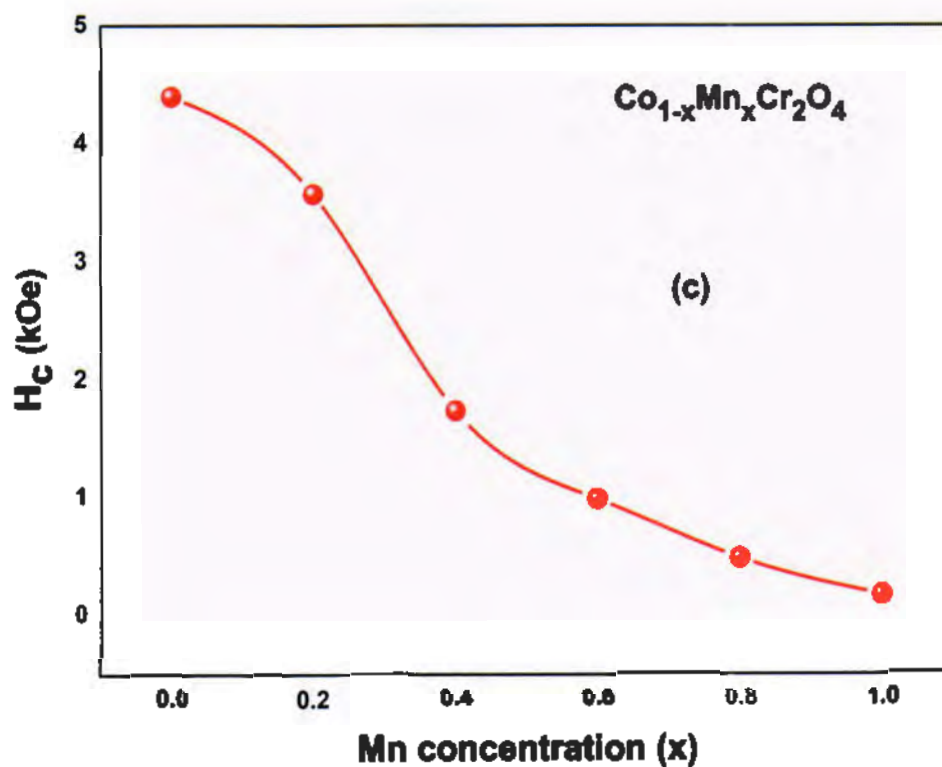


Fig. 4.5: (a) M- H Loops of $\text{Co}_{1-x}\text{Mn}_x\text{Cr}_2\text{O}_4$ nanoparticles (b) Variation of saturation magnetization (M_s) and (c) coercivity (H_c) with different Mn concentration (x). In (b) and (c), line just shows the trend.

Conclusion

The magnetic properties of Mn doped CoCr_2O_4 nanoparticles with $x = 0, 0.2, 0.4, 0.6, 0.8$ and 1 compositions were analysed briefly. The Sol-gel method was used for preparation of these nanoparticles. XRD showed that all the prepared nanoparticles have normal cubic spinel structure. No impurity was found which assures single phase $\text{Co}_{1-x}\text{Mn}_x\text{Cr}_2\text{O}_4$ nanoparticles. TEM images revealed cubic like shape of MnCr_2O_4 nanoparticles and also agglomeration due to magnetic nature. FTIR showed octahedral and tetrahedral transmission bands which confirmed the spinel structure of these nanoparticles. These bands shifted toward lower wavenumber with Mn doping. ZFC/FC curve of CoCr_2O_4 nanoparticles showed the paramagnetic to ferrimagnetic phase transition takes place at $T_C = 100$ K, Spin spiral state at $T_S = 30$ K and finally lock-In transition state appeared at $T_L = 10$ K. Doping of Mn in CoCr_2O_4 nanoparticles shifted the all magnetic transitions towards low temperatures and finally MnCr_2O_4 showed T_C at 54 K with antiferromagnetic transition at $T_N = 20$ K. M-H loops of Mn doped CoCr_2O_4 nanoparticles showed an increasing trend in saturation magnetization due to high magnetic moment of Mn as compared to Co and decreasing trend in coercivity due to high value of magnetocrystalline anisotropy of Co as compared to Mn with increasing concentration of Mn.

References:

- [1] Chemistry.tutorvista.com/inorganic-chemistry/solid-state.html.
- [2] T. Shinjo, Nanomagnetism and Spintronics, Elsevier Science, 2013.
- [3] B.D. Cullity, C.D. Graham, Introduction to Magnetic Materials, Wiley, 2009.
- [4] J.M.D. Coey, Magnetism and Magnetic Materials, Cambridge University Press, 2004.
- [5] T.L.Francavilla, R.A. Hein, D.H. Liebenberg, Magnetic susceptibility of superconductors and other spin systems, Springer Science & Business Media, 2013.
- [6] C. Mullins, Magnetic susceptibility of the soil and its significance in soil science a review, *Eur. J. Soil Sci.* **28** (1977) 223-246.
- [7] V. Iacovacci, G. Lucarini, L. Ricotti, A. Menciassi, Magnetic Field-Based Technologies for Lab-on-a-Chip Applications, in: Lab-on-a-Chip Fabrication and Application, InTech, 2016.
- [8] C. Heck, Magnetic materials and their applications, Elsevier, 2013.
- [9] A. Abragam, B. Bleaney, Electron Paramagnetic Resonance of Transition Ions, by A. Abragam and B. Bleaney, 1970.
- [10] N.A. Spaldin, Magnetic materials: fundamentals and applications, Cambridge University Press, 2010.
- [11] F. Martín-Hernández, E.C. Ferré, Separation of paramagnetic and ferrimagnetic anisotropies: A review, *J. Geophys. Res.: Solid Earth* **112** (2007).
- [12] Z.-F. Guo, K. Pan, X.-J. Wang, Electrochromic & magnetic properties of electrode materials for lithium ion batteries, *Chin Phys. B* **25** (2015) 017801.
- [13] G. Rangarajan, Materials science, Tata McGraw-Hill Education, 2004.
- [14] D. Jiles, Introduction to magnetism and magnetic materials, CRC press, 2015.
- [15] A.G. Arani, Z.K. Maraghi, A feedback control system for vibration of magnetostrictive plate subjected to follower force using sinusoidal shear deformation theory, *Ain Shams Eng. J.* **7** (2016) 361-369.
- [16] T. Moriya, Nuclear magnetic relaxation near the Curie temperature, *Prog. Theor. Phys.* **28** (1962) 371-400.
- [17] S. Zollner, T.N. Nunley, D.P. Trujillo, L.G. Pineda, L.S. Abdallah, Temperature-dependent dielectric function of nickel, *Appl. Surf. Sci.* (2016).
- [18] D.R. Askeland, W.J. Wright, Essentials of materials science & engineering, Cengage Learning, 2013.

- [19] E. Motovilova, S. Huang, *Magnetic Materials for Nuclear Magnetic Resonance and Magnetic Resonance Imaging*, (2017).
- [20] L. Maxwell, What is ferrimagnetism?, *Electrical Engineering*, **73** (1954) 804-806.
- [21] M. Singh, *Engg Physics*, McGraw-Hill Education (India) Pvt Limited.
- [22] D.-T. Ngo, *Lorentz TEM characterisation of magnetic and physical structure of nanostructure magnetic thin films*, 2017.
- [23] D. Askeland, P. Fulay, W. Wright, *The science and engineering of materials*, Nelson Education, 2011.
- [24] A. Akbarzadeh, M. Samiei, S. Davaran, *Magnetic nanoparticles: preparation, physical properties, and applications in biomedicine*, *Nanoscale. Res. Lett.* **7** (2012) 144.
- [25] D.C. Jiles, D.L. Atherton, *Theory of ferromagnetic hysteresis*, *J. Magn. Magn. Mater.* **61** (1986) 48-60.
- [26] F. Peinado, E. Medel, R. Silvestre, A. Garcia, *Open-grade wearing course of asphalt mixture containing ferrite for use as ferromagnetic pavement*, *Composites Part B: Eng.* **57** (2014) 262-268.
- [27] R.N. Sinn, *Dekker encyclopedia of nanoscience and nanotechnology*, *Reference & User Services Quarterly*, **44** (2005) 257-259.
- [28] M.F. Hochella, *Nanoscience and technology: the next revolution in the Earth sciences*, *Earth. Planet. Sci. Lett.* **203** (2002) 593-605.
- [29] N. Tolochko, *History of nanotechnology*, *Nanoscience and nanotechnology. Encyclopaedia of life Support Systems (EOLSS)*, Developed under the auspices of the UNESCO, SEolss Published, oxford, (2009).
- [30] *The different dimensions of nanotechnology*, *Nat. Nanotech.* **4** (2009) 135.
- [31] S.M. Naidu, *Applied Physics*, Pearson Education India, 2009.
- [32] X. Han, S. Li, Z. Peng, A.-R. Obeed Al-Yuobi, A. Saieh Omar Bashammakh, M.S. El-Shahawi, R. Leblanc, *Interactions between Carbon Nanomaterials and Biomolecules*, 2016.
- [33] F.H. Khan, *Chemical hazards of nanoparticles to human and environment (a review)*, *O.J. Chem.* **29** (2014) 1399-1408.
- [34] M. Kamran, A. Ullah, S. Rahman, A. Tahir, K. Nadeem, M.A. ur Rehman, S. Hussain, *Structural, magnetic, and dielectric properties of multiferroic $\text{Co}_{1-x}\text{Mg}_x\text{Cr}_2\text{O}_4$ nanoparticles*, *J. Magn. Magn. Mater.* **433** (2017) 178-186.

- [35] M. Kamran, A. Ullah, Y. Mehmood, K. Nadeem, H. Krenn, Role of SiO₂ coating in multiferroic CoCr₂O₄ nanoparticles, *AIP Advances*, **7** (2017) 025011.
- [36] Z. Ristanovic, A. Kalezic-Glisovic, N. Mitrovic, S. Djukic, D. Kosanović, A. Maricic, The Influence of Mechanochemical Activation and Thermal Treatment on Magnetic Properties of the BaTiO₃FexOy Powder Mixture, 2015.
- [37] C. Rath, P. Mohanty, A. Banerjee, Magnetic properties of nanoparticles of cobalt chromite, *J. Magn. Magn. Mater.* **323** (2011) 1698-1702.
- [38] Y. Yamasaki, S. Miyasaka, Y. Kaneko, J.-P. He, T. Arima, Y. Tokura, Magnetic reversal of the ferroelectric polarization in a multiferroic spinel oxide, *Phys. Rev. Lett.* **96** (2006) 207204.
- [39] N. Menyuk, K. Dwight, A. Wold, Ferrimagnetic spiral configurations in cobalt chromite, *J. Phys.* **25** (1964) 528-536.
- [40] M. Ptak, M. Maćzka, K. Hermanowicz, A. Pikul, J. Hanuza, Particle size effects on the magnetic and phonon properties of multiferroic CoCr₂O₄, *J. Solid State Chem.* **199** (2013) 295-304.
- [41] S. Lei, L. Liu, C. Wang, X. Shen, C. Wang, D. Guo, S. Zeng, B. Cheng, Y. Xiao, L. Zhou, A facile in situ reduction route for preparation of spinel CoCr₂O₄ polycrystalline nanosheets and their magnetic properties, *Cryst. Eng. Comm.* **16** (2014) 277-286.
- [42] B.C. Melot, J.E. Drewes, R. Seshadri, E. Stoudenmire, A.P. Ramirez, Magnetic phase evolution in the spinel compounds Zn_{1-x}Co_xCr₂O₄, *J. Phys.: Condense. Matter.* **21** (2009) 216007.
- [43] Z. Lu, J. Zhu, E. Andrew Payzant, M.P. Paranthaman, Electrical conductivity of the manganese chromite spinel solid solution, *J. Am. Ceram. Soc.* **88** (2005) 1050-1053.
- [44] L. Chang, D. Huang, W. Li, S. Cheong, W. Ratcliff, J. Lynn, Crossover from incommensurate to commensurate magnetic orderings in CoCr₂O₄, *J. Phys.: Condense. Matter.* **21** (2009) 456008.
- [45] J.K. Galivarapu, D. Kumar, A. Banerjee, C. Rath, Magnetic Transitions in Chemically Synthesized Nanoparticles of CoCr₂O₄, *IEEE. T. Magn.* **52** (2016) 1-6.
- [46] M. Edrissi, A.R. Keshavarz, Synthesis of cobalt chromite nanoparticles by thermolysis of mixed Cr³⁺ and Co²⁺ chelates of 2-mercaptopyridin N-oxide, *Nano-Micro Lett.* **4** (2012) 83-89.

- [47] M. Akyol, İ. Adanur, A.O. Ayaş, A. Ekicibil, Magnetic field dependence of magnetic coupling in CoCr_2O_4 nanoparticles, *Physica B: Condense. Matter.* **525** (2017) 144-148.
- [48] Z. Tian, C. Zhu, J. Wang, Z. Xia, Y. Liu, S. Yuan, Size dependence of structure and magnetic properties of CoCr_2O_4 nanoparticles synthesized by hydrothermal technique, *J. Magn. Magn. Mater.* **377** (2015) 176-182.
- [49] X. Chen, Z. Yang, Y. Xie, Z. Huang, L. Ling, S. Zhang, L. Pi, Y. Sun, Y. Zhang, Coexistence of incommensurate and commensurate spiral orders and pressure effect on polycrystalline CoCr_2O_4 , *J. Appl.Phys.* **113** (2013) 17E129.
- [50] M. Kamran, K. Nadeem, M. Mumtaz, Negative and anomalous T-dependent magnetization trend in CoCr_2O_4 nanoparticles, *Solid State Sci.* **72** (2017) 21-27.
- [51] I. Sosnowska, W. Schäfer, W. Kockelmann, K. Andersen, I. Troyanchuk, Crystal structure and spiral magnetic ordering of BiFeO_3 doped with manganese, *Appl. Phys. A*, **74** (2002) 1040-1042.
- [52] P. Choudhary, D. Varshney, Structural, vibrational and dielectric behavior of $\text{Co}_{1-x}\text{M}_x\text{Cr}_2\text{O}_4$ (M= Zn, Mg, Cu and $x= 0.0, 0.5$) spinel chromites, *J. Alloy Compd.* **725** (2017) 415-424.
- [53] M. Younis, M. Saleem, S. Atiq, S. Naseem, Magnetic phase transition and magneto-dielectric analysis of spinel chromites: MCr_2O_4 (M = Fe, Co and Ni), *Ceram. Int.* (2018).
- [54] X. Chen, H. Zhang, C. Wang, X. Luo, P. Li, Effect of particle size on magnetic properties of zinc chromite synthesized by sol–gel method, *Appl. Phys. Lett.* **81** (2002) 4419-4421.
- [55] S.A. Gene, E. Saion, A.H. Shaari, M.A. Kamarudin, N.M. Al-Hada, A. Kharazmi, Structural, optical, and magnetic characterization of spinel zinc chromite nanocrystallines synthesised by thermal treatment method, *J. Nanomater* **15** (2014).
- [56] S. Li, G. Zhao, H. Bi, Z. Huang, H. Lai, R. Gai, Y. Du, Synthesis and anomalous magnetic properties of CoCr_2O_4 nanocrystallites with lattice distortion, *J. Magn. Magn. Mater.* **305** (2006) 448-451.
- [57] K. Dwight, N. Menyuk, J. Feinleib, A. Wold, Reduced Manganese Moment in Manganese Chromite, *J. Appl. Phys.* **37** (1966) 962-963.
- [58] T. Tsakalagos, I.A. Ovid'ko, A.K. Vasudevan, *Nanostructures: synthesis, functional properties and application*, Springer Science & Business Media, 2012.

- [59] V.M. Rotello, *Nanoparticles: building blocks for nanotechnology*, Springer Science & Business Media, 2004.
- [60] V. Pareek, A. Bhargava, R. Gupta, N. Jain, J. Panwar, *Synthesis and Applications of Noble Metal Nanoparticles: A Review*, *Advanced Science, Engineering and Medicine*, **9** (2017) 527-544.
- [61] C. Suryanarayana, M.G. Norton, *X-ray diffraction: a practical approach*, Springer Science & Business Media, 2013.
- [62] A.G. Ghom, *Textbook of Oral Radiology-E-Book*, Elsevier Health Sciences, 2017.
- [63] G. Cao, Y. Wang, *Nanostructures and nanomaterials: synthesis, properties, and applications*, World Scientific, 2004.
- [64] P. John, *Textbook of oral medicine*, JP Medical Ltd, 2014.
- [65] O.E. Langland, R.P. Langlais, J.W. Preece, *Principles of dental imaging*, Lippincott Williams & Wilkins, 2002.
- [66] R.L. Myers, *The basics of physics*, Greenwood Publishing Group, 2006.
- [67] B. Basu, *Biomaterials Science and Tissue Engineering: Principles and Methods*, Cambridge University Press, 2017.
- [68] H. Moynihan, A. Crean, *Physicochemical Basis of Pharmaceuticals*, Oxford University Press, 2009.
- [69] H. Alipooramirabad, A. Paradowska, R. Ghomashchi, A. Kotousov, M. Reid, *Quantification of residual stresses in multi-pass welds using neutron diffraction*, *J. Mater Process. Techn.* **226** (2015) 40-49.
- [70] H. Abudayyeh, *Synthesis and Analysis of ZnO Nanowires*, 2012
- [71] *Engineering Physics(for Anna University)*, 1/e, Pearson Education.
- [72] B.C. Smith, *Fundamentals of Fourier transform infrared spectroscopy*, CRC press, 2011.
- [73] J. Clarke, A.I. Braginski, *The SQUID Handbook: Fundamentals and Technology of SQUIDs and SQUID Systems*, Wiley, 2004.
- [74] J.F. Annett, *Superconductivity, superfluids and condensates*, Oxford University Press, 2004.
- [75] V. In, A. Palacios, *Symmetry in Complex Network Systems: Connecting Equivariant Bifurcation Theory with Engineering Applications*, Springer, 2017.
- [76] D. Feng, G. Jin, *Introduction to condensed matter physics*, World Scientific, 2005.
- [77] A.I. Figueroa, *Magnetic Nanoparticles: A Study by Synchrotron Radiation and RF Transverse Susceptibility*, Springer, 2014.

- [78] C.H.C. Giraldo, Evidence of Superconductivity in the magnetic properties of specially prepared Palladium hydride and deuteride.
- [79] J. Wecker, G. Bayreuther, G. Ross, R. Grössinger, *Magnetic Properties*, 2011.
- [80] H.g. Zhang, W.h. Wang, E.k. Liu, X.d. Tang, G.j. Li, H.w. Zhang, G.h. Wu, Compensation effect and magnetostriction in $\text{CoCr}_{2-x}\text{Fe}_x\text{O}_4$, *Phys. Status solidi (b)*, **250** (2013) 1287-1292.
- [81] O. Udalov, N. Chtchelkatchev, I. Beloborodov, Electric field control of magnetic properties and magneto-transport in composite multiferroics, *J. Phys: Condense. Matter*. **27** (2015) 186001.
- [82] M. Maćzka, M. Ptak, M. Kurnatowska, J. Hanuza, Synthesis, phonon and optical properties of nanosized CoCr_2O_4 , *Mater. Chem. Phys.* **138** (2013) 682-688.
- [83] D. Gingasu, I. Mindru, D.C. Culita, L. Patron, J.M. Calderon-Moreno, P. Osiceanu, S. Preda, O. Oprea, V. Parvulescu, V. Teodorescu, Structural, magnetic and catalytic properties of cobalt chromite obtained through precursor method, *Mater. Res. Bullet.* **62** (2015) 52-64.
- [84] D.P. Dutta, J. Manjanna, A. Tyagi, Magnetic properties of sonochemically synthesized CoCr_2O_4 nanoparticles, *J. Appl. Phys.* **106** (2009) 043915.
- [85] A. Afzal, S. Atiq, M. Saleem, S.M. Ramay, S. Naseem, S.A. Siddiqi, Structural and magnetic phase transition of sol-gel-synthesized Cr_2O_3 and MnCr_2O_4 nanoparticles, *J.Sol-Gel Sci. Tech.* **80** (2016) 96-102.
- [86] Y. Zhou, Z. Yang, L. Li, Y. Xie, S. Lin, Y. Sun, Y. Zhang, Magnetic field and external pressure effects on the spiral order of polycrystalline MnCr_2O_4 , *J. Magn. Magn. Mater*, **324** (2012) 3799-3801.
- [87] Y. Köseoğlu, F. Alan, M. Tan, R. Yilgin, M. Öztürk, Low temperature hydrothermal synthesis and characterization of Mn doped cobalt ferrite nanoparticles, *Ceram. Int.* **38** (2012) 3625-3634.
- [88] R. Choubey, D. Das, S. Mukherjee, Effect of doping of manganese ions on the structural and magnetic properties of nickel ferrite, *J. Alloy. Compds.* **668** (2016) 33-39.
- [89] V. Torgashev, A. Prokhorov, G. Komandin, E. Zhukova, V. Anzin, V. Talanov, L. Rabkin, A. Bush, M. Dressel, B. Gorshunov, Magnetic and dielectric response of cobalt-chromium spinel CoCr_2O_4 in the terahertz frequency range, *Phys. Solid State.* **54** (2012) 350-359.